Applied Surface Science 659 (2024) 159919

Contents lists available at ScienceDirect

Applied Surface Science

journal homepage: www.elsevier.com/locate/apsusc

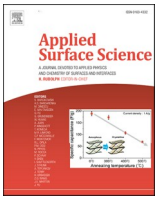

Full Length Article

Formation of Li-Al LDH conversion layer on AA2024 alloy for corrosion protection

Jules Stephan [a,1], Valeryia Kasneryk [b,*,1], Maria Serdechnova [b], Nico Scharnagl [b], Eugen Gazenbiller [b], Bahram Vaghefinazari [b], Polina Volovitch [a], Maksim Starykevich [c], Carsten Blawert [b], Mikhail L. Zheludkevich [b,d,e]

[a] Chimie ParisTech, PSL University, CNRS, Institut de Recherche de Chimie Paris (IRCP), 11 Rue Pierre et Marie Curie, 75005 Paris, France
[b] Institute of Surface Science, Helmholtz-Zentrum Hereon, Max-Planck-Straße 1, 21502 Geesthacht, Germany
[c] Department of Materials and Ceramic Engineering, CICECO - Aveiro Institute of Materials, University of Aveiro, 3810-193 Aveiro, Portugal
[d] Faculty of Engineering, CAU Kiel University, Kaiserstraße 2, 24143 Kiel, Germany
[e] Kiel Nano, Surface and Interface Science (KiNSIS), Kiel University, Christian-Albrechts-Platz 4, D-24118 Kiel, Germany

ARTICLE INFO

Keywords:
AA2024 alloy
Layered double hydroxide
Corrosion protection
Conversion coating
Cu complexation
Chelating agent

ABSTRACT

AA2024 aluminium alloy is widely used in the aerospace industry. However, it is known to be highly susceptible to localised corrosion, which is related to its complex microstructure, mainly the presence of numerous Cu-rich intermetallic particles. One of the effective solutions to increase their corrosion resistance relies on the formation of layered double hydroxide (LDH) based conversion coatings (CC). This investigation aims to understand how the conditions of *in situ* Li-Al LDH-CO_3^{2-}/OH^- CC growth affect their further protective ability. For that purpose, concentration of reactants (0.05–0.15 M Li_2CO_3), pH of the electrolyte (10–12), temperature (30–50 °C) and treatment time (15 min-30 h) were systematically varied. Additionally to that, NH_4OH was applied as a chelating agent for the synthesis of Li-Al LDH-CO_3^{2-}/OH^- as well as for the pH control. The obtained protective coatings were evaluated by X-ray diffraction (XRD), scanning electron microscopy (SEM), glow discharge optical emission spectroscopy (GDOES), Raman spectroscopy, salt spray test (SST) and electrochemical impedance spectroscopy (EIS). Among all varied parameters, involvement of chelating agent was found to be the most efficient for the formation of a coating with the highest level of corrosion protection. This is attributed to the formation of soluble complexes between NH_4OH and Cu, resulting in dissolution of the intermetallics. It also prevents further redeposition of Cu species and consequently, the formation of new highly active Cu cathodes on the AA2024 alloy surface.

1. Introduction

Nowadays, aluminium and its alloys found a broad application in aeronautic industry. Such interest can be explained by a good compromise between low density and mechanical properties [1]. Among different Al based alloys, AA2024 is mostly used due to its high strength and fracture toughness, good damage tolerance and lower structural weight. However, AA2024 is highly prone to corrosion due to its complex microstructure and presence of numerous intermetallic particles containing copper [2]. The intermetallic particles create microgalvanic couples with the alloy matrix [3], providing sites for corrosion initiation and propagation, which leads to dealloying process [4,5]. Due to this, the corrosion protection of AA2024 becomes extremely important.

One of the most effective ways to enhance corrosion resistance of metallic surfaces is based on application of conversion coatings. They are used to reduce reactivity by limiting the diffusion of the electrolyte to the metal, i.e. acting as a physical barrier. Moreover, they are excellent adhesion promoters for further applications of polymer coatings or paints [6]. In the past, aeronautical manufacturers used substantially chromate-containing coatings. Their excellent protective behaviour was related to "self-healing" Cr (VI) properties, which refers to their ability to recover in the damaged areas [7–9]. Moreover, chromates are also known to suppress dealloying and trenching in aluminium alloys [3]. However, their biggest disadvantage is high

* Corresponding author.
E-mail address: valeryia.kasneryk@hereon.de (V. Kasneryk).
[1] These authors contributed to the work equally and should be regarded as co-first authors.

https://doi.org/10.1016/j.apsusc.2024.159919
Received 2 February 2024; Received in revised form 1 March 2024; Accepted 15 March 2024
Available online 17 March 2024

toxicity and harmful impact on the environment and human health [10] and the use of Cr(VI) is now under restrictions of REACH. Due to these reasons, the use of chromate based coatings is strongly restricted and they are planned to be fully banned in the nearest future [11]. Therefore, numerous studies are now focused on the development of new environmental friendly corrosion protection methods with the aim to replace chromate-based coatings [12].

Over the past several years, among various other surface treatments, layered double hydroxide (LDH) conversion coatings have attracted a lot of attention. They are known for their excellent properties like physical barrier, ion-exchange properties, and environmental-friendly aspect [7,13]. LDHs belong to the class of anionic clays with hydrotalcite-like structures [7,14]. LDHs are typically composed of positively-charged mixed metal M^{I}/M^{II}–M^{III} hydroxide layers and interlayers occupied by anions (A^{y-}) and water molecules. The general formula of the most common LDHs can be represented as $[M^{II}_{1-x}M^{III}_{x}(OH)_2]^{x+}(A^{y-})_{x/y}]\bullet zH_2O$ [15,16]. In corrosion protection strategies, the LDHs act as smart "nanocontainers", i.e. they release intercalated functional compounds on demand in the presence of corrosive species. Moreover, due to their ability to be intercalated with high amount of inhibitors, LDHs can provide long-term corrosion protection [7,17,18].

LDH based CC have already demonstrated their effectiveness for corrosion protection of AA2024 alloy. In that context, Zn-Al LDH CC were mostly in focus of the investigations. Tedim et al. developed a 2-step method for preparation of Zn-Al LDH coatings, which was based on an *in situ* growth of Zn-Al LDH-NO_3^- on the surface of AA2024 followed by further intercalation of VO_x^- ions [19–22]. As alternative to vanadate, intercalation of molybdate and 2-mercaptobenzothiazole (MBT) into Zn-Al LDH also can improve corrosion resistance of AA2024 substrate [23–25]. In all these cases, high level of protection was explained by the release of the inhibitors from the LDH based CC. The released inhibitors can further suppress dealloying of the intermetallic particles and decrease the reduction of oxygen, as it was demonstrated for vanadates anions [26,27]. Or they can form insoluble products representing additional physical barrier as in the case of MBT or molybdate [28,29]. However, in spite of enhanced corrosion protection, there are still several drawbacks considering further application of Zn-Al LDH based CC, especially on the industrial level. The first one relates to relatively high temperatures used for their preparation. Thus, in most of the investigations effective *in situ* growth of Zn-Al LDH was achieved only under temperatures higher than 70 °C. Another problem relates to the tendency of Zn-Al LDH to crystallise into "flower"-like zones, i.e. leading to an inhomogeneous covering of the AA2024 surface with flakes, as it was demonstrated in [30]. Moreover, the performance of Zn-Al LDH still did not reach the level of the chromate based CC, even in combination with further post-treatments including sol-gels [31,32] or hydrophobic molecules (i.e. hexadecyltrimetoxisilane [24]).

Significantly less studied Li-Al LDH CCs represent an alternative to Zn-Al LDH CCs for corrosion protection of AA2024 aluminium alloy. Already in 1994, Buchheit et al. reported that the treatment of aluminium alloys (AA1100, AA2024-T3, AA6061-T6, AA7075-T6) with aqueous solution of lithium carbonate at room temperature significantly improved their corrosion resistance [33]. It was attributed to the formation of hydrotalcite compound with a composition of $Li_2[Al_2(OH)_6]_2{\cdot}CO_3{\cdot}nH_2O$, which was expected to provide barrier protection of metallic surfaces. From that time, Li-Al LDH demonstrated their effectiveness for corrosion protection of different Al based substrates. It can be exemplified by Li-Al LDH CC intercalated with aspartic acid [34], disodium vanillin L-aspartic acid [35] or methionine [36], which provided self-healing and barrier protection of AA6N01 [34,35] or AA6063 [36] alloys. Moreover, Li-Al LDH in combination with superhydrophobic treatments (1,1,2,2-perfluorodecyltrimethoxysilane or 1,1,2,2-perfluorooctyltriethoxysilane) were reported to improve corrosion and wetting resistance of AA2099-T83 [37], AA2198-T851 [38] and AA6N01 Al [39] alloys.

Additionally, another Li-Al LDH feature must be mentioned. Relatively mild conditions of Li-Al LDH growth allows its *in situ* formation on the surface of Al based alloys during corrosion process. This was discovered by Visser et al., who investigated corrosion processes taking place on the surface of AA2024 coated with organic coatings, where lithium based salts (namely, $Li_2C_2O_4$ or Li_2CO_3) were applied as fillers. Li-Al LDH was *in situ* formed by Li^+ leached from the coating and Al^{3+} dissolved from the alloy, enabling a system with self-healing ability [40–44].

Meanwhile, regardless the significant effort done in the development of Li-Al LDH CC for corrosion protection of different Al based substrates, there is still a lack of understanding how the conditions of the *in situ* LDH growth affect the protective ability of the coating. This article focuses on the effect of NH_4OH as a chelating agent and other synthesis conditions (concentration of treating agent (Li_2CO_3), duration, pH, temperature of the bath) on the structure and anticorrosion properties of the formed Li-Al LDH-CO_3^{2-}/OH^- conversion coatings.

2. Experimental part

2.1. Materials

2.1.1. Substrate

As substrate for the current work, AA2024 aluminium alloy with the following nominal composition according to spark analysis (Spectrolab M9, Ametek-Spectro, Germany) was used (Table 1).

The samples were cut into 2 cm x 3 cm and 3 cm x 4 cm plates. Prior to the LDH growth, the specimens were ground with #1200 and #2500 grades of silicon carbide paper, rinsed with deionized water and finally dried at 25 °C under free air conditions.

2.1.1.1. Reactants. Lithium carbonate (≥99.0 %, Sigma Aldrich), sodium carbonate (≥98.0 %, Carl Roth), sodium hydroxide (≥99.0 %, Carl Roth), ammonium hydroxide (28–30 wt%, Thermo Fisher Scientific), nitric acid (100 %, Merck) were used for the LDH growth.

2.1.1.2. Synthesis of Li-Al LDH-CO_3^{2-}/OH. Solutions with specific concentration of Li_2CO_3 (0.05 M, 0.1 M, 0.15 M) were prepared. Such concentrations were chosen based on the knowledge about lithium carbonate solubility, which is 1.32 g/100 ml H_2O at 30 °C and 1.18 g/100 ml H_2O at 50 °C [45], and in agreement with the conditions applied before for the formation of Li-Al LDH-CO_3^{2-}/OH^- on various Al based substrates [33,37]. After complete dissolution of lithium carbonate, pH of the respective solutions was adjusted using a 1 M NaOH solution or 2 M HNO_3 to 10.0, 10.5, 11.5, 12. The obtained solutions were then heated to 30 °C or 50 °C. After the particular temperature was reached, AA2024 specimens were immersed into the solution for particular times, t (15 min, 1 h, 3 h, 5 h, 16 h, 24 h and 30 h) under continuous stirring. Impact of the chelating agent was studied by addition of 28–30 % NH_4OH solution till the pH value reached 11.5. All tested conditions are presented in Table 2. After the treatment, the samples were finally rinsed with deionized water for several times and dried at 25 °C under air conditions. In the paper, the samples are named as c–pH–T–t in the text and figures, where c represents concentration of lithium carbonate used, pH – corresponding pH, T – temperature of the treatment and t – treatment time. Samples obtained in the presence of NH_4OH were titled as c–pH–T–t–NH_4OH.

2.2. Characterisation of the formed coatings

Phase composition of each specimen was verified by X-ray diffraction (XRD) using D8 Advanced Powder diffractometer (Bruker, Germany; Ni-filtered Cu Kα radiation). The measurements were carried out under following settings: a glancing angle of 3°, a scan range from 5 till 65°, a step size of 0.02°, a scan speed of 1 s or 10 s per step.

The phase composition of Li-Al LDH films on aluminium substrate

Table 1
Nominal composition of used AA2024 in wt% (analysed by spark analysis).

Component	Al	Cu	Fe	Cr	Mg	Mn	Si	Ti	Zn	Others
wt%	93.18	4.65	0.085	0.023	1.42	0.44	0.095	0.031	0.04	0.03

Table 2
Conditions tested for the synthesis of Li-Al LDH- CO_3^{2-}/OH^-.

Variable parameter	Concentration	pH	Temperature
Synthesis conditions	**0.1 M** Li_2CO_3, pH **11.5, 30 °C**, time: 15 min – 30 h		
	0.05 M Li_2CO_3, pH 11.5, 30 °C, 15 min – 30 h	0.1 M Li_2CO_3, pH **10.5**, 30 °C, 15 min – 30 h	0.1 M Li_2CO_3, pH 11.5 **50 °C**, 15 min – 30 h
	0.15 M Li_2CO_3, pH 11.5 30 °C, 15 min – 30 h	0.1 M Li_2CO_3, pH **11**, 30 °C, 15 min – 30 h	
		0.1 M Li_2CO_3, pH **12**, 30 °C, 15 min – 30 h	
	0.1 M Li_2CO_3, pH **11.5 (NH_4OH), 30 °C**, time: 15 min – 30 h		

was also studied at the P08 high-resolution diffraction beamline from the PETRA III synchrotron radiation source (DESY, Hamburg, Germany) with an X-ray energy of 25 KeV with incident angle value of 0.12° θ and exposure time of 1 s. A two-dimensional PERKIN Elmer detector with a pixel size of 200 μm was used.

Surface morphology and cross-sections of obtained samples were analysed using a Tescan Vega3 SB scanning electron microscope (SEM, Czech Republic) equipped with an energy dispersive X-ray spectrometer (EDS, Ultim Max 40 Oxford, UK). Morphology of the samples was analysed in secondary electrons (SE) mode, while cross section views were observed in back scattered electrons (BSE) UniVac mode. Acquisition was done with high voltage of 8.0–12.0 kV and beam intensity of 7.0–12.0. Before analysis of cross-sections, the specimens were embedded in resin and then ground through successive grades of silicon carbide paper (#800, #1200, #2500, #4000) and then washed with deionized water. The size of the LDH flakes was estimated using ImageJ program.

A glow discharge optical emission spectroscopy (GDOES) depth profile analysis of the obtained coatings was performed using a GD-Profiler 2 (HORIBA, France) at an operating pressure of 650 Pa and a power of 30 W using a 4 mm anode. The following spectrum lines were employed: Al at 396.152 nm, C at 165.701 nm, Li at 670.791 nm, Cu at 324.754 nm, H at 121.567 nm, and O at 130.217 nm.

Further structure analysis was done by Raman spectroscopy using a confocal Raman microscope (Bruker, Senterra, Germany). All data acquisition was performed at 532 nm laser wavelength, 20 × objective lens, 25 mW laser power, 50 μm aperture size, and 64 scans with an integration time of 2 s. Raman spectral data were evaluated using Bruker OPUS 7.5.18 software.

Thermodynamic calculations of the possibility of LDH formation on the surface of AA2024 aluminium alloy were performed using Hydra-Medusa software version of 18 Aug. 2009. Stability constants of all complexes were taken from the Hydra database from Jun. 2015 [46]. Simulations were done under following parameters: ionic strength I = 2 mol/(kg H_2O), temperature t = 25 °C and concentrations c (Li^+) = 200 mM, c (CO_3^{2-}) = 100 mM, c (Al^{3+}) = 0.10 mM, c (NH_3) = 15 mM.

Initial corrosion characterisation was performed by salt spray test (SST). The test was carried out using 5 wt% NaCl solution at 35 °C in a salt spray test chamber SC/KWT 450 (Weiss Umwelttechnik GmbH, Germany) according to ASTM B117 standard. The images of the specimens after SST were recorded using a Canon EOS 760D optical camera. The area of the corrosion-affected surface was estimated from the obtained photos using ImageJ program. Moreover, samples after SST were evaluated by XRD and SEM. Furthermore, electrochemical impedance spectroscopy (EIS) was performed for additional characterisation. It was done in a naturally aerated 3.5 wt% NaCl solution at 25 °C for 7 days of immersion. Measurements were conducted with a Gamry 1000 potentiostat (USA) using a conventional three-electrode cell, employing a platinum counter electrode, a saturated Ag/AgCl electrode and the working electrode was the respective LDH CC layer or bare AA2024 alloy (exposed area 0.5 cm^2). Analysis was over a frequency range from 100 kHz to 0.01 Hz at open circuit potential (OCP), with 10 mV RMS sinusoidal potential perturbations. Each type of the specimen was measured for three times to test reproducibility of the performance. After 7 days of the EIS measurements, samples were characterised by SEM. The impedance spectra were fitted with ZView software, version 3.3c (Scribner, North Carolina, USA).

3. Results and discussion

3.1. Li-Al LDH-CO_3^{2-}/OH^- CC: Condition for growth

Prior to synthesis, appropriate pH range for Li-Al LDH-CO_3^{2-}/OH^- formation was estimated via thermodynamic calculations using Hydra-Medusa software [46]. The results of the simulation for the syntheses in the presence of NaOH or NH_4OH are presented in Fig. 1. Both plots demonstrate similar equilibrium compositions. As it can be seen from Fig. 1, a, b, CO_3^{2-} needed for the formation LDH phase is the predominant anion among other carbonate species in the pH range from 10.5 till 14, while at lower pH values high amount of HCO_3^- and H_2CO_3 species can be present in the solutions. Li^+ is expected to be present in high amount at pHs from 7 till 13, after which its concentration slightly decreases. Moreover, LiOH concentration gradually increases with a pH growth from 7 till 13. Additionally, soluble $LiNH_3^+$ is present in the NH_4OH containing solution at pH = 10–13 (Fig. 1, b). Presence of soluble Li^+, $LiNH_3^+$ and LiOH is advantageous as all these species can take part in the formation of LDH structure [47,48]. Al^{3+} is delivered into the solution upon dissolution of AA2024 alloy, which at high pHs forms $Al(OH)_3$, crystallised $Al(OH)_3$ and $Al(OH)_4^-$. Among these species, $Al(OH)_4^-$ becomes a dominating one at the pH = 10.5–14. Being soluble, $Al(OH)_4^-$ can be easily rearranged and participate in the formation of the LDH, similarly to one presented in [49,50]. Summarising all mentioned aspects, it can be concluded that the pH values starting from 10.5 can be proposed as optimum for effective Li-Al LDH-CO_3^{2-}/OH^- growth for both NaOH and NH_4OH containing solutions. However, as it was demonstrated in [48,51], the high level of AA2024 substrate dissolution can take place at pH > 12, which is undesirable. Due to that reason, pHs from 10.5 till 12 were in focus.

3.2. Impact of the treatment conditions on Li-Al LDH-CO_3^{2-}/OH^- CC growth

In order to understand how conditions of the Li-Al LDH-CO_3^{2-}/OH^- CC growth affect its following protective ability, concentration of lithium carbonate, pH, temperature and treatment time were systematically varied. The formation of LDH coatings on the surface was firstly followed by XRD (Fig. 2). (0 0 2) and (0 0 4) diffraction reflections (located at 11.6 and 23.1° 2θ), which are typical for the LDH structure ($Li_2Al_4(CO_3)(OH)_{12}{\cdot}3H_2O$), were visible for most of the patterns.

The first parameter of the synthesis, which was systematically varied, was the concentration of lithium carbonate in the treatment bath. Its variation under pH = 11.5 showed, that it has a minor impact on the LDH crystallisation (Fig. 2, a). Even at the lowest concentration of lithium carbonate (0.05 M), Li-Al LDH-CO_3^{2-}/OH^- phase was formed as

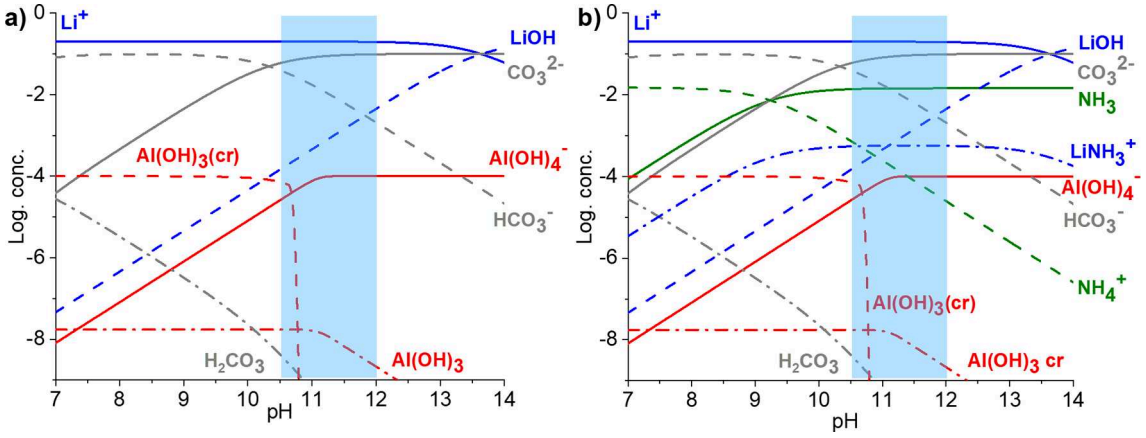

Fig. 1. Thermodynamic calculation of the equilibrium composition in the solution containing a) c (Li^+) = 200 mM, c (CO_3^{2-}) = 100 mM, c (Al^{3+}) = 0.10 mM and b) c (Li^+) = 200 mM, c (CO_3^{2-}) = 100 mM, c (Al^{3+}) = 0.10 mM and c (NH_3) = 15 mM. Al^{3+} is a main product of dissolution of AA2024 alloy.

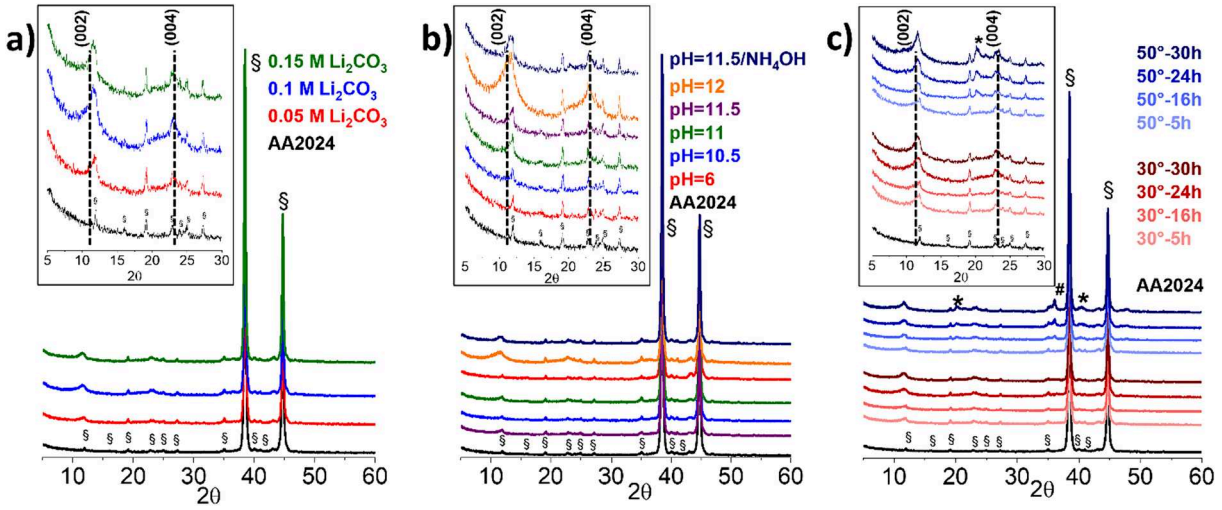

Fig. 2. XRD patterns of Li-Al LDH-CO_3^{2-}/OH^- CC grown on the surface of AA2024 aluminium alloy at different conditions. a) Variation of Li_2CO_3 concentration at pH = 11.5, 30 °C for 24 h. b) Variation of pH for the syntheses from the bath containing 0.1 M Li_2CO_3 at 30 °C for 24 h. c) Variation of time and temperature for the syntheses from the reaction bath containing 0.1 M Li_2CO_3 at pH = 11.5. *-$Al(OH)_3$ and #-$5Al_2O_3{\cdot}H_2O$ admixture phases, §-AA2024 alloy.

the LDH reflections were observed in the XRD pattern (Fig. 2, a, red). With increase of the concentration of lithium carbonate to 0.15 M, the reflections of LDHs became broader and more intensive than for the concentrations of 0.1 M and 0.05 M. It indicates the presence of a higher amount LDH crystals on the surface and their possible disorder. Moreover, it can be related to possible small crystals size as well as nanocrystalline nature.

Variation of the pH in the reaction bath demonstrated that no significant effect on the LDH crystallisation was observed by the XRD measurements for the specimens obtained at pH 10.5–11.5 (Fig. 2, b). Further increase of pH till 12 resulted in the increase of the intensity and broadening of the reflections corresponding to the Li-Al LDH phase. Similarly to variation of Li_2CO_3 concentration, it can also be related to the increase of the amount of LDH flakes on the surface and their enlargement. Application of the Bragg formula confirmed, that this LDH was characterised by the highest interlamellar spacing among all specimens, namely 7.70 Å, while it was 7.68 Å for 0.1–11.5–30–24 (Table SI-1). Additionally, in order to understand if Li-Al LDH phase can be formed on the surface of AA2024 even at lower pH, synthesis at pH = 6.0 (pH was decreased by nitric acid) was also performed. Under the conditions applied, no presence of LDH phase was detected. Actually, pKa1 of CO_2/HCO_3^- is equal to 6.4. While decreasing the pH, most of carbonate can leave the reaction mixture by production of CO_2 gas. Consequently, with a lower concentration of carbonate, conversion of the surface was not possible. Additionally, the impact of the pH on the formation of the Li-Al LDH phase was studied using Raman spectroscopy (*Fig. SI-1*). All specimens were characterized by the presence of bands at 1065 cm^{-1}, 585 cm^{-1} and 350 cm^{-1}, which are typical for LDH with carbonate ions inside the intergalleries [30,52–55]. They are related to the symmetrical stretching of CO_3^{2-} molecules linked by hydrogen interaction to interlayer water molecules or OH^-. The signals located in the range of 3000–3600 cm^{-1} are associated with vibrations of OH^- and H_2O. The 150 cm^{-1} band presented on all spectra corresponds to vibration of Me-O bonds. Moreover, the weak band at 480 cm^{-1} in the spectra of the 0.1–**11.5**–30–24 (*Fig. SI-1*, b) and 0.1–**12**-30–24 (*Fig. SI-1*, c) specimens can be related to the asymmetric and symmetric stretch mode of the bonding between Cu and OH, indicating deposition of Cu species on the surface during the coating formation. It must be mentioned that, while for the specimens obtained under the pH 11.5 and 12 (with NaOH), these signals have high intensity, the one for the sample prepared under the pH = 10.5 were less intensive and broader, which was most likely relate to the presence of lower amount of LDH on the surface.

Increase of the treatment temperature stronger affected Li-Al LDH-CO_3^{2-}/OH^- formation. First, the XRD patterns of the LDHs synthesized from 0.1 M Li_2CO_3 at 50 °C and pH 11.5 (Fig. 2, c) show the reflection peaks of LDH with enhanced intensity. This difference, as it was also

confirmed by the results of SEM (chapter 3.3), was related to the increase of the LDH flakes size. Moreover, the LDH crystallisation at 50 °C was accompanied by the formation of $Al(OH)_3$ and $5Al_2O_3{\cdot}H_2O$ admixture phases. The XRD pattern of the specimens obtained at elevated temperature demonstrated the signals at 35.8 (#, $5Al_2O_3{\cdot}H2O$), 20.3 and 40.5° 2θ (*, $Al(OH)_3$), in contrast to the specimens obtained at 30 °C representing single LDH phase. In parallel to the parameters discussed previously, treatment time was also systematically varied from 15 min till 30 h. Independently on the applied conditions, Li-Al LDH film starts to grow on the surface of AA2024 alloy only after 1 h of treatment as it can be seen from the XRD patterns for 0.1–11.5–30–t (*Fig. SI-2*). The intensity of the (0 0 2) reflection slightly increased with prolongation of the treatment time, but no principal differences were observed in the patterns of the specimens treated for 24 h or 30 h, as it can be seen from the XRD patterns of the specimens treated with 0.1 M Li_2CO_3 at pH = 11.5 and 30 °C and 50 °C presented in Fig. 2, c.

Additionally, in order to control the process of Cu redistribution on the surface of AA2024 alloy, the Li-Al LDH growth was also carried out in the presence of ammonia hydroxide as a chelating agent, which at the same time controlled the pH value. NH_4OH was chosen based on numerous reported investigations [18,30,56,57]. It was demonstrated that aqueous NH_3 present in the Zn-Al LDH synthesis bath could form various complexes with copper leached from the substrate. Such complexation prevents further Cu redistribution on the alloy surface and consequently improves the corrosion performance [57]. Moreover, NH_3 itself can facilitate dissolution of Cu from intermetallic particle. In turn, it results in the change of local pH, which can favour a strong dissolution of the Al substrate and consequently accelerate LDH formation [30]. Similar phenomenon was detected for the Li-Al LDH-CO_3^{2-}/OH^- crystallisation on the surface of AA2024 (Fig. 2, b). The XRD pattern of the specimen obtained with 0.1 M Li_2CO_3 at pH = 11.5 at 30 °C for 24 h in the presence of NH_4OH demonstrates a bit more intensive signals corresponding to the LDH phase comparing to the one obtained under the same conditions with NaOH, which is clearly seen from *Fig. SI-3* representing comparison of both patterns. It confirms the presence of higher amount of LDH phase on the surface of substrate material. Raman spectrum (*Fig. SI-1*) of the samples also confirms the formation of Li-Al LDH-CO_3^{2-}/OH^- CC on the surface of AA2024.

As facilities of the laboratory XRD are limited for determination of the minor phases in the coatings, detailed phase composition of the Li-Al LDH coating was performed using XRD with synchrotron radiation. The typical XRD pattern (namely, for 0.1–11.5–30–24 specimen) is presented in Fig. 3. As it can be seen, only Li-Al LDH structure was formed on the surface of AA2024 alloy. The diffraction reflections at 8.2, 14.5, 15.2, 15.8, 16.7, 24.5, 25.4° 2θ, which are typical for the $Li_2Al_4(CO_3)(OH)_{12}{\cdot}3H_2O$ phase, are clearly visible in the pattern. Additionally, the presence of native oxide phase can be also detected in the XRD pattern. The corresponding reflections of Al_2O_3 are located at 17.7, 19.3, 22.3, 22.7 and 25.6° 2θ. The other signals in the region from 5 till 30° 2θ belong to the initial AA2024 aluminium alloy.

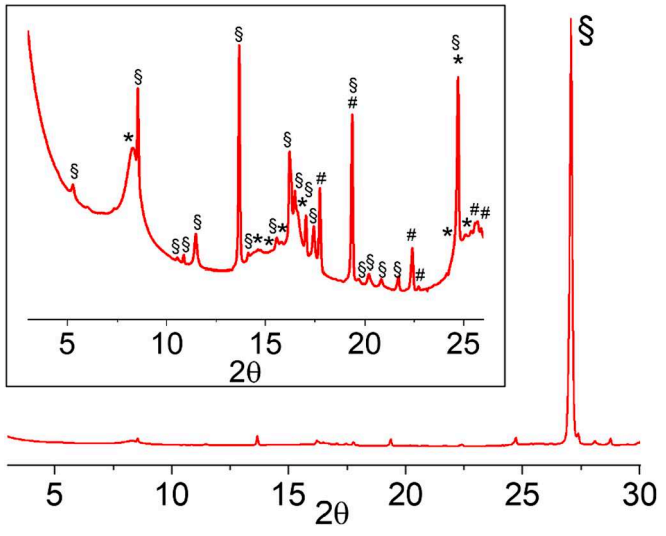

Fig. 3. Synchrotron X-ray diffraction pattern for Li-Al LDH-CO_3^{2-}/OH^- (obtained in 0.1 M Li_2CO_3, pH = 11.5 at 30 °C for 24 h). The inset shows magnification of the low angle region of the pattern. *-$Li_2Al_4(CO_3)(OH)_{12}{\cdot}3H_2O$, #-$Al_2O_3$, §-AA2024.

3.3. Surface morphology and element distribution

As the structure differences by XRD were observed mainly for the **0.15**–11.5–30–24, 0.1–**12**–30–24, 0.1–11.5–**50**–24 and 0.1–11.5–30–24–**NH_4OH** specimens, these coatings were in focus of further characterisation. 0.1–11.5–30–24 was analysed to compare the effect of treatment conditions. Fig. 4 represents the photos and SEM micrographs of the obtained coatings. The Li-Al LDH-CO_3^{2-}/OH^- coating grown for 24 h at 30 °C and pH 11.5 (Fig. 4, a, b) exhibits homogeneous covering of the surface with LDH flakes. These results also correlate with the EDS elemental mapping presented in Fig. 5 showing homogenous distribution of Al and O on the surface, which are main elements forming LDH structure. Moreover, as it can be seen, presence of Cu intermetallics is also visible on the upper surface, some of them were agglomerated (Fig. 4, b, Fig. 5).

Variation of conditions for *in situ* LDH growth including increase of Li_2CO_3 concentration, pH and temperature was not effective for the formation of uniform Li-Al LDH coating on the surface of AA2024. Photos and SEM images of the **0.15**–11.5–30–24 and 0.1–11.5–**50**–24 (Fig. 4, d, e and k, l, respectively) specimens show that less homogenous coatings were formed on the surface of AA2024 aluminium alloy comparing to 0.1–11.5–30-24. Moreover, in contrast to 0.1–11.5–30–24, no intermetallic particles were visible on the upper surface of the both coatings based SEM images. It was related to the formation of dense Li-Al LDH layer above the intermetallics. However, their presence can be followed from EDS elemental distribution of Cu (Fig. 5).

Synthesis at pH = 12 was also not effective for the formation of uniform Li-Al LDH-CO_3^{2-}/OH^- CC on the surface of AA2024 aluminium alloy (Fig. 4, g). Firstly, SEM micrograph (Fig. 4, h) demonstrates the presence of high amount of agglomerated intermetallic particles on the surface. Based on the EDS mappings, these particles were enriched with Cu. It can be proposed that they were formed during the process of redistribution of Cu on the surface, which was leached from Cu-rich intermetallic particles [58–60], similarly to one observed during the Zn-Al LDH-NO_3^- formation on the surface of AA2024 alloy [57]. The mechanism of Cu redistribution is discussed in SI. Presence of such insoluble Cu-rich species on the surface is crucial as they represent highly efficient Cu cathodes and consequently favour corrosion processes [61]. Moreover, the surface of 0.1–**12**–30–24 contained numerous cracks. As it can be seen from EDS elemental mapping, the areas with high concentration of Al were located between cracks, indicating exposure of AA2024 surface. Such areas provide easy access for the aggressive mediate to the substrate interface and consequently can also accelerate the corrosion processes.

Based on visual inspection, the most homogenous coverage of the AA2024 aluminium alloy surface with Li-Al LDH layer was achieved when NH_4OH was added into the reaction bath (Fig. 4, m). Meanwhile, the SEM image (Fig. 4, n) demonstrates the presence of particle on the upper surface of Li-Al LDH CC, which are mainly composed of Cu based on EDS mappings (Fig. 5). However, their amount and size were significantly smaller in comparison to the coatings obtained without adding the chelating agent. Such observation is associated with dissolution of intermetallics facilitated by NH_4OH and formation of soluble complexes of Cu as it was discussed previously.

Concerning effect of the conditions for *in situ* LDH growth on the LDH flake morphology, no variation of pH or addition of the chelating agent

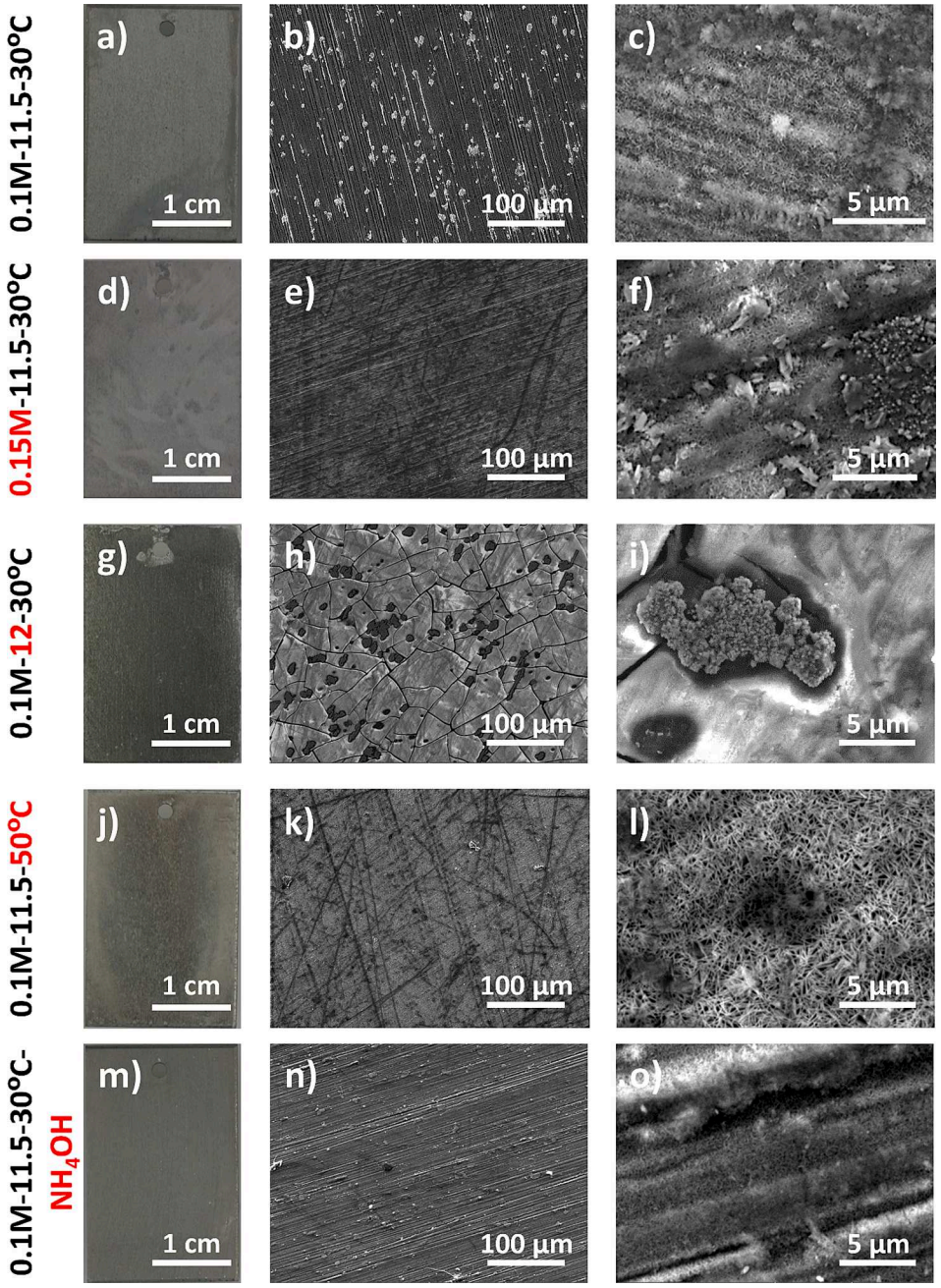

Fig. 4. Photos and SEM micrographs of AA2024 samples covered with a)-b) 0.1–11.5–30–24; d)-e) **0.15**–11.5–30–24; g)-h) 0.1–**12**–30–24; j)-k) 0.1–11.5–**50**-24 and m)-n) 0.1–11.5–30–24–**NH_4OH** specimens. c), f), i), l), o) represents the high-magnification pictures for the coatings, respectively.

(NH_4OH) had a significant effect on the LDH crystals size. Thus, 0.1–11.5–30–24, 0.1–**12**–30–24 and 0.1–11.5–30–24–**NH_4OH** specimens were characterised by the flake size length of approximately 100–200 nm (Fig. 4, c, i, o). In all three cases nanoflakes were grown mostly vertically to the substrate. Additionally, areas with horizontal orientation of the flakes were also detected for 0.1–11.5–30–24. Such orientation of the flakes can be considered as advantageous as it provides higher coverage of the surface, and thus, potentially can improve the barrier protection of the coating similarly to that reported previously for Ni-Al LDH-CO_3^{2-} [62]. In contrast, the LDH flakes were non-uniform with a size varied from 0.2 to 2 µm in case of the specimen prepared from the reaction mixture containing 0.15 M Li_2CO_3. Moreover, the LDH crystals were disordered on the surface and exhibited both vertical and horizontal orientation.

In agreement with the XRD data, the highest impact on the LDH crystals morphology was detected when the temperature increased to 50 °C. Micrograph of LDH grown at 50 °C (Fig. 4, k)) depicts big differences in the crystal size compared to other conditions discussed previously. The length of the flakes was around 1 µm, i.e. 10 times bigger than for LDH grown under the same synthesis parameters at 30 °C. The coating was uniform and was characterised mainly by vertical orientation of the flakes in contrast to the specimen obtained at the same conditions at 30 °C, as it can be seen from Fig. 4, l) and Fig. 5. Based on the analysis of the cross sections (Fig. SI-4), the coating was dense with a thickness around 2.5–3 µm, while for 0.1–11.5–30-24 this value reached only 1.2 µm. EDS mappings of cross section confirmed homogenous distribution of Al and O through the entire coatings.

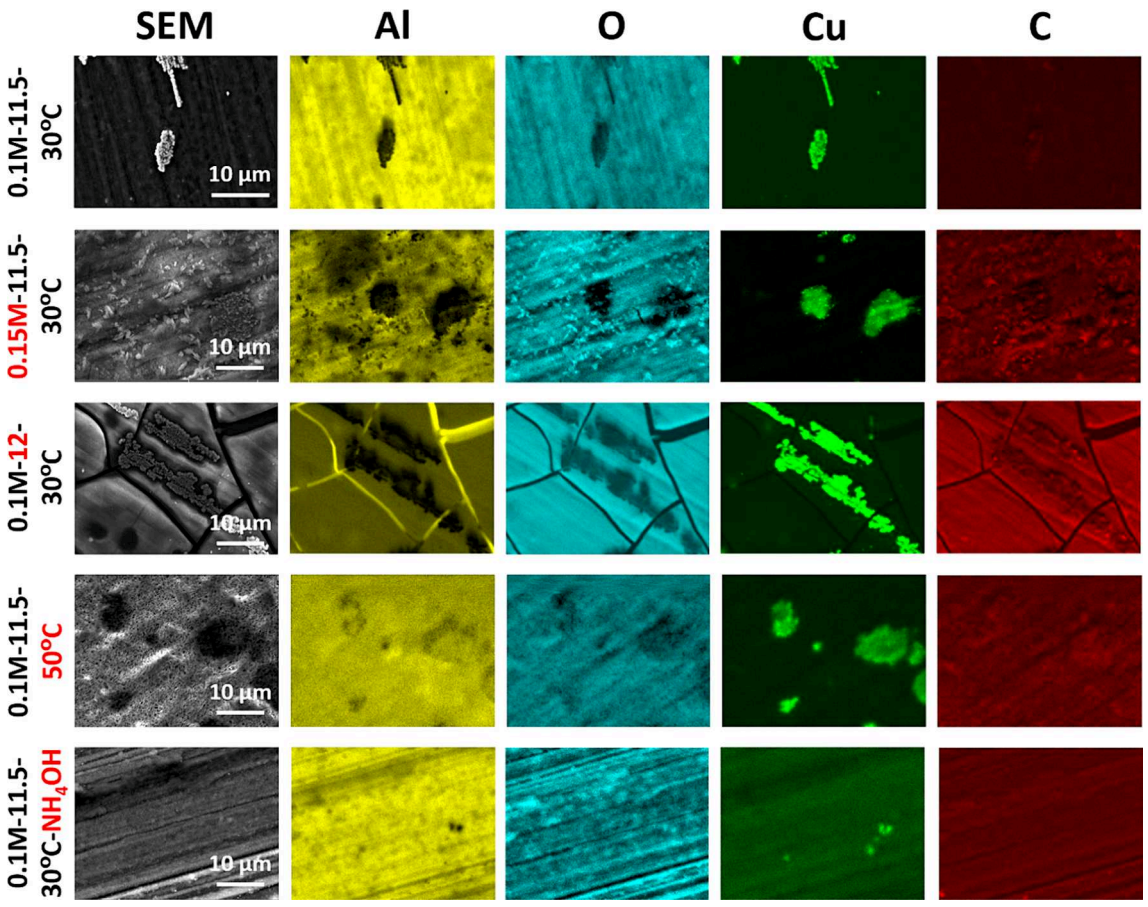

Fig. 5. EDS mapping results of Li-Al LDH-CO_3^{2-}/OH^- grown on the surface of AA2024: 0.1–11.5–30–24, **0.15**–11.5–30–24, 0.1–**12**–30–24, 0.1–11.5–**50**–24 and 0.1–11.5–30–24–**NH_4OH** specimens.

3.4. Analysis of elemental in depth distribution through the coating by GDOES

Glow discharge optical emission spectroscopy (GDOES) depth profile analysis was performed to understand how the conditions applied for the growth of Li-Al LDH-CO_3^{2-}/OH^- CC affect the elemental distribution across the layer thickness. The coating thicknesses can also be estimated by following the element composition. The 0.1–11.5–30–24, 0.1–11.5–**50**–24 and 0.1–11.5–30–24–**NH_4OH** specimens were studied as they represented the most homogenous coatings by SEM and EDS.

Depth profiles of selected LDH coatings obtained under different conditions are shown in Fig. 6. The specimens obtained at 30 °C were characterised by the comparable etching time, while the one obtained at 50 °C erodes approximately 3 times longer, considering similar erosion rate of the layers for different samples. It can be interpreted by the difference in layers thickness and by the enlargement of LDH flakes for the samples obtained under higher temperature demonstrated by SEM and cross sections (Fig. 4, *Fig. SI-4*). In case of all three specimens, presence of two regions are seen (for better visibility they are marked with vertical dash lines). The first region, where the C, Li, and O signals were highly intensive, corresponds to the area of Li-Al LDH coating (region I). After Li-Al LDH CC reaches the aluminium based substrate (region II), the intensity of the signal corresponding to aluminium as the main component of the substrate starts to rise, which is accompanied by the drop of the intensity of other signals down to the background level. It must be pointed out that high intensities of carbon during the first seconds of etching can be attributed to the contamination of the surface by absorbed CO_2. Interestingly, the intensity of Li increases close to the interface between the LDH layer and the substrate. This result agrees with the data reported by Kosari et al. demonstrating the formation of dense Li-containing pseudoboehmite phase close to interface, when Li_2CO_3 was used as an additive for polyurethane coating applied for the protection of AA2024 aluminium alloy [42,63]. Moreover, previous studies demonstrated that lithium can be inhomogeneously distributed through the entire LDH coating [63]. Similar observation was done from the spectrum of lithium for Li-Al LDH-CO_3^{2-}/OH^- CC grown on the surface of AA2024 in the presence of chelating agent. It demonstrates the presence of an intensive peak in the middle area of the coating indicating inhomogeneous distribution of Li inside the LDH coating.

Finally, the impact of chelating agent on the spectra of Cu must be also mentioned. Fig. 6, d represents the comparison of Cu signals for the specimens discussed previously. The 0.1–11.5–**50**–24 specimen was characterised by presence of lower amount of Cu in the area of the coating (region I) comparing to the 0.1–11.5–30–24 one (Fig. 6, c, a, respectively), indicating that the increase of the temperature of the synthesis facilitated Cu dissolution from AA2024 alloy. However, the highest impact was detected for the specimen obtained in the presence of chelating agent, as the intensity of Cu signals was significantly decreased for the 0.1–11.5–30–24–**NH_4OH** comparing to other two specimens (Fig. 6, b). It could be related to the fact, that in the presence of ammonium in the reaction bath, Cu ions released from the intermetallic particles remain mainly in the reaction bath in the form of soluble complexes $Cu(NH_3)_x^{2+}$. In turn, Cu can be redistributed on the surface, when the synthesis takes place without involvement of chelating agent, similar to the reported for the growth of Zn-Al LDH [57].

3.5. Corrosion performance

In order to understand how conditions of the Li-Al LDH-CO_3^{2-}/OH^- growth affect their protective ability, the specimens were firstly

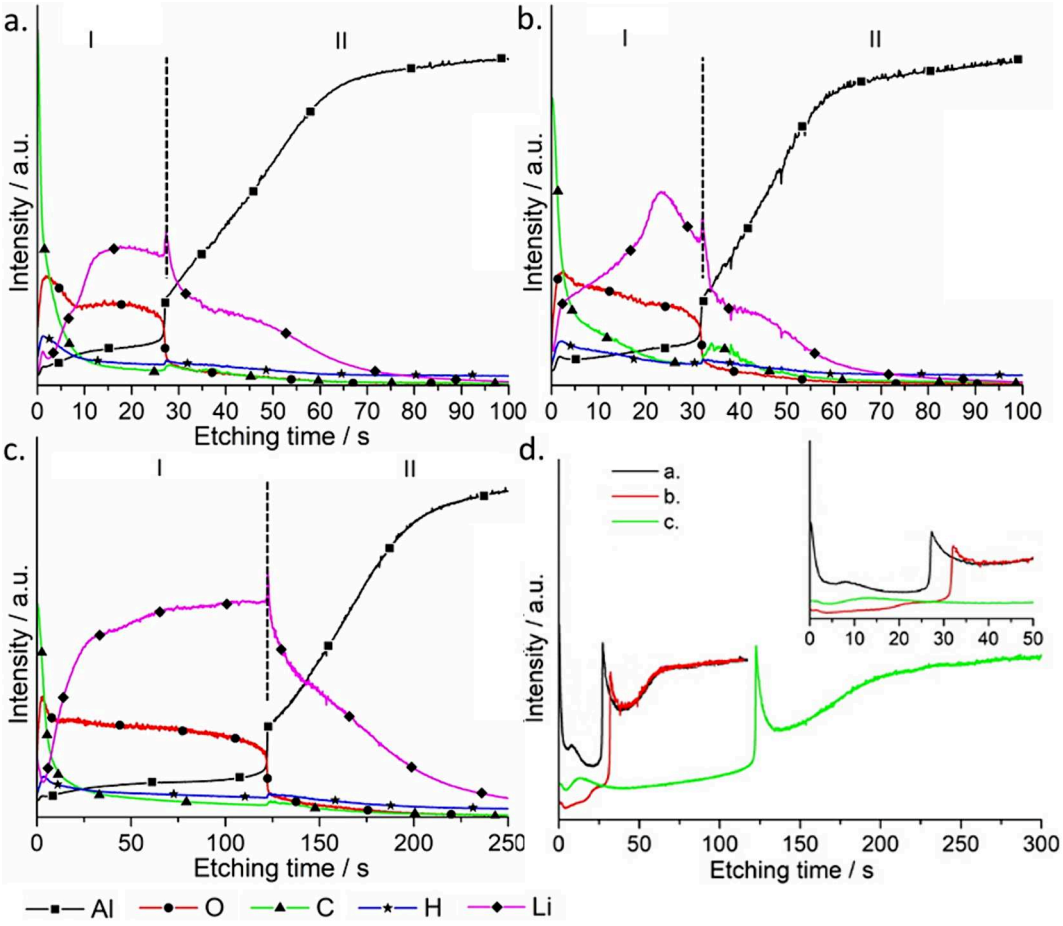

Fig. 6. GDOES depth profile of AA2024 samples coated with Li-Al LDH-CO_3^{2-}/OH^- a) 0.1–11.5–30–24; b) 0.1–11.5–30–24–**NH_4OH**; c) 0.1–11.5–**50**–24; d) GDOES depth profile for Cu for a. 0.1–11.5–30–24, b. 0.1–11.5–30–24–**NH_4OH** and c. 0.1–11.5–**50**–24.

subjected to salt spray test. Fig. 7 represents the photos of bare AA2024 alloy and 0.1–11.5–30–24, **0.15**–11.5–30–24, 0.1–**12**–30–24 h, 0.1–11.5–**50**–24, 0.1–11.5–30–24–**NH_4OH** subjected to SST for 4, 24, 48 and 164 h. The Table SI-2 represents the values of corroded surfaces estimated from the photos using ImageJ program.

The bare AA2024 alloy was corroding fast and demonstrated the presence of high amount of corrosion products on the surface. 24 % of surface area has been already corroded after 4 h of exposure and this value increased to 67 % with prolongation of the experiment from 4 till 168 h. The specimens obtained in 0.1 M and 0.15 M Li_2CO_3 (pH = 11.5, 30 °C) solutions demonstrated a behaviour comparable to bare AA2024. Even after 4 h of exposure they have been highly corroded confirming that concentration of lithium carbonate applied for Li-Al LDH formation does not principally affected the corrosion protection of final coating. In turn, the increase of the bath pH was crucial for the protective ability of Li-Al LDH CC. The specimen prepared at pH = 12 demonstrated the lowest protection ability, which was even worse that for bare AA2024 alloy. Thus, around 32 % of the surface has been already damaged after 4 h of the treatment and further prolongation of the exposure led only to an increase of the amount of the surface corrosion products. Such behaviour of the 0.1–**12**–30–24 sample correlates with the data of SEM demonstrated the presence of numerous cracks and agglomerations of active intermetallics on the surface.

An increase of temperature for Li-Al LDH CC growth positively affected its protective ability, as the samples obtained under 50 °C were characterised only by 2 % of damaged surface after 4 h of SST. Moreover, while bare AA2024 plates and specimens obtained with variation of the pH and Li_2CO_3 concentration were fully corroded after 24 h, the 0.1–11.5–**50**–24 specimen was corroded only after 168 h. Such behaviour can be explained by the formation of thicker LDH layer demonstrated by the cross sections (*Fig. SI-4*), and consequently, formation of more effective physical barrier on the surface comparing to the specimens obtained at 30 °C.

Among all the specimens, the highest level of protection was observed for that synthesised in the presence of NH_4OH as a chelating agent. The first signs of corrosion were detected on the plate's surface only after 48 h of the exposure and were estimated as 1.4 %. Even after 168 h of the SST, the specimen showed the presence of the lowest amount of corrosion products comparing to the other plates coated with Li-Al LDH-CO_3^{2-}/OH^-. While specimens obtained under standard conditions (i.e. without application of the chelating agent) were fully corroded after 168 h of exposure, the sample with 0.1–11.5–30–24–NH_4OH CC exhibited only 7.4 % of corroded surface area. In order to further evaluate stability of Li-Al LDH CC prepared in the presence of chelating agent, the coatings were prepared on the surface of AA2024 alloy with a size of 3 x 4 cm and also tested by SST for 816 h. The results are presented in SI (*Fig. SI-5*). The larger specimen demonstrated comparable behaviour to the presented in Fig. 7. But prolongation of the exposure demonstrated that the specimen was fully corroded after 336 h of SST. The sample exposed for 816 h demonstrated the presence of high amount of corrosion products as well as numerous pits on the surface.

Further evaluation of protective properties of Li-Al LDH-CO_3^{2-}/OH^- CC obtained in the presence of NH_4OH chelating agent was performed by electrochemical impedance spectroscopy measurements. The performance was compared for the samples prepared with or without NH_4OH. Bare AA2024 aluminium alloy was used as a reference. Fig. 8 represents the Bode plots for the specimens after 1 h, 24 h and 168 h of

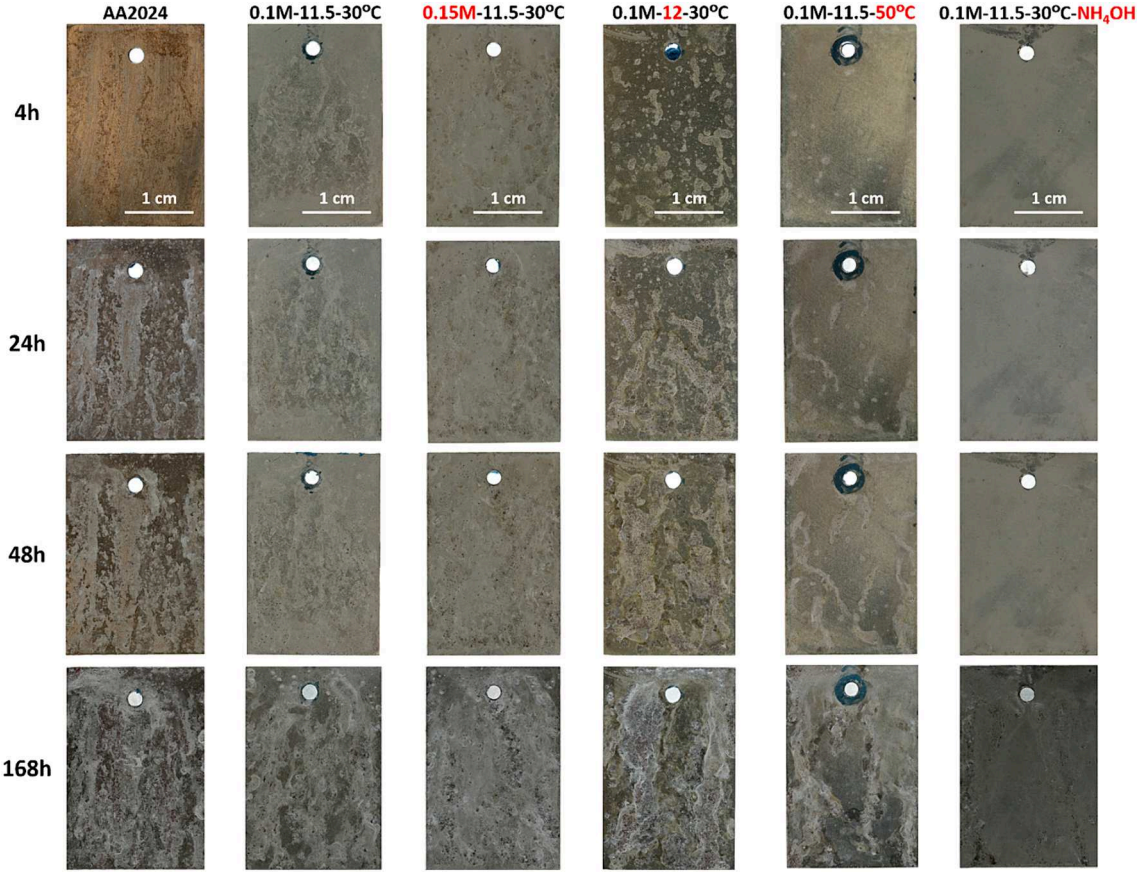

Fig. 7. Photographs of bare AA2024 aluminium alloy and specimens covered with Li-Al LDH-CO_3^{2-}/OH^- CC under different condition (treatment for 24 h) and subjected to salt spray test during different times.

immersion into 3.5 wt% NaCl solution. The total impedance modulus |Z| at low frequencies (Fig. 8, a, c, e) for the specimen obtained in the presence of the chelating agent had the highest value. *Fig. SI-6* shows the evolution of |Z| at 0.01 Hz as a function of time during the whole immersion. The highest values of the low frequency impedance for all immersion times were up to 1 order of magnitude higher compared to bare AA2024 plate or the one coated with Li-Al LDH-CO_3^{2-}/OH^- CC obtained without NH_4OH. The same trend remained even after immersion into 3.5 wt% NaCl solution for 168 h. Moreover, analysis of the literature data for other types of LDH CC grown on the surface of AA2024 alloy (Table SI-4) confirmed that the performance of 0.1–11.5–30–24–**NH_4OH** was comparable or even superior than Zn-Al-LDH, Zn-Al-Ce-LDH or Ca-Al-LDH [19–21,25,64–66].

The EIS spectra of most samples (Fig. 8) demonstrate the presence of several relaxation processes. Due to a strong overlapping, the time constants cannot always be easily resolved, especially for the Li-Al LDH-CO_3^{2-}/OH^- CC prepared with chelating agent (after 1 h of EIS testing). After 1 h of immersion, two relaxation processes can be detected in the spectra of all specimens (Fig. 8, a,b). The first one located at approximately 10 Hz is attributed to the presence of native oxide layer on the surface of bare alloy surface. In turn, the low-frequency time constant at 0.1 Hz is associated with electrochemical activities on the alloy surface. In the case of the Li-Al LDH-CO_3^{2-}/OH^- CC obtained in the presence of NH_4OH, there is an additional time constant visible at the higher frequencies (about 1 kHz) which is originated from a weak barrier response of the LDH layer. However, this layer did not provide long-term stability and fully disappeared after 4 h of immersion (SI, *Fig. SI-7*).

The impedance spectra were fitted using equivalent circuits to obtain the quantitative characterisation of the samples performance. The equivalent circuits used to fit the spectra are represented in Fig. 9 as well as an example of the fitting of the experimental data. While most of the EIS spectra were fitted with equivalent circuit b), for the spectrum of the specimens obtained in the presence of NH_4OH after one hour of exposition, the equivalent circuit c) was applied. For the equivalent circuits, R_s corresponds to the solution resistance, CPE_{ox} and R_{ox}, CPE_l and R_l are associated with capacitance and resistance of natural oxide layer on the surface and additional protective layer, respectively, CPE_{dl} is the double layer capacitance of the electrolyte/metal interface and R_{ct} is charge transfer resistance across it. The obtained quantitative parameters obtained based on the analysis of the EIS spectra (Fig. 8) are presented in SI, Table SI-3. Experimental data were reasonably fitted with chi-squared values in the range of 0.01–0.001. Li-Al LDH-CO_3^{2-}/OH^- CC obtained with an addition of the chelating agent demonstrated the highest values of R_{ox} among with minimum values of CPE_{ox}, thus also confirming that this coating provides the highest corrosion resistance of the aluminium substrate.

3.5.1. *Analysis of the corroded specimens*

Finally, the specimens after EIS and SST tests were evaluated by the XRD and SEM and EDS. The results are presented in Fig. 10, Fig. 11, *Fig. SI-8*, *Fig. SI-9*, *Fig. SI-10* and *Fig. SI-11*. Based on SEM, the specimen coated with Li-Al LDH-CO_3^{2-}/OH^- CC in the presence of NH_4OH was significantly less corroded that the one obtained without chelating agent or bare AA2024 plate (Fig. 10, *Fig. SI-8*). Higher amount of corrosion products was deposited on the surface of bare AA2024 alloy and specimen coated with 0.1–11.5–30–24. Moreover, corrosion pits can also be detected on the surface of Li-Al LDH-CO_3^{2-}/OH^- CC obtained without NH_4OH. EDS mappings of the top view and cross sections of the specimens after 168 h of EIS presented in Fig. SI-10 and Fig. SI-11 exhibit inhomogeneous distribution of Al, O, and Cl elements on the surface for

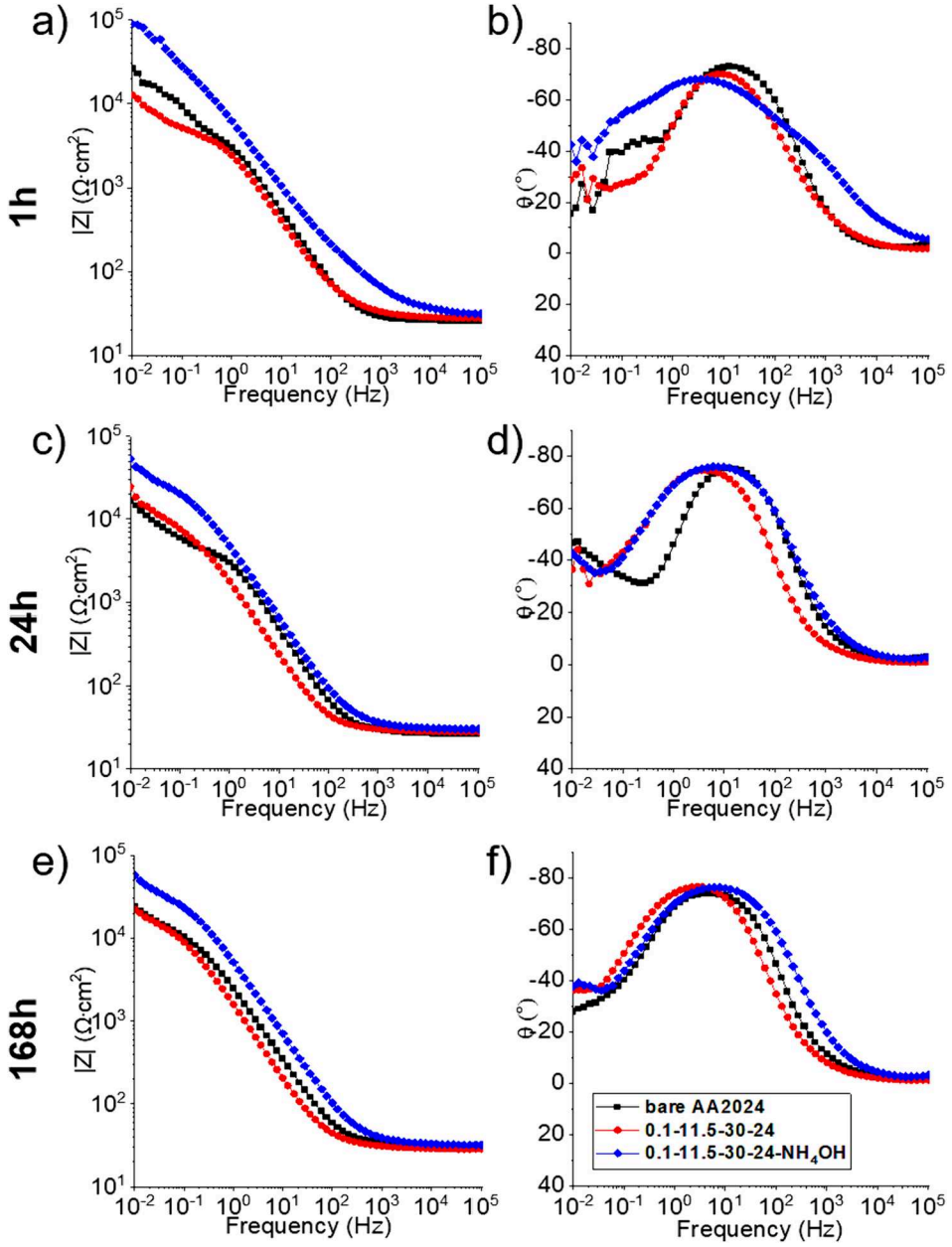

Fig. 8. Bode (a, c, e) and phase angle (b, d, f) plots for bare AA2024 aluminium alloy (black), and coated with Li-Al LDH-CO_3^{2-}/OH^- under following conditions: 0.1 M Li_2CO_3 at pH = 11.5 at 30 °C for 24 h (red); 0.1 M Li_2CO_3 at pH = 11.5 at 30 °C for 24 h in the presence of NH_4OH (blue) after 1 h, 24 h and 168 h of the immersion into 3.5 wt% NaCl solution at 25 °C. (For interpretation of the references to colour in this figure legend, the reader is referred to the web version of this article.)

all three specimens. Moreover, deposition of the corrosion products around Cu-rich intermetallics was detected for the 0.1–11.5–30–24–NH_4OH, which correlates with a cross section analysis confirming propagation of the corrosion around Cu-rich intermetallics. Comparing cross sections of three specimens after EIS, corrosion was less propagated in case of the 0.1–11.5–30–24–NH_4OH. XRD patters of the corroded Li-Al LDH-CO_3^{2-}/OH^- CC specimens demonstrate that the main corrosion product was $Al(OH)_3$ (bayerite) phase, as the reflections at 18.3 and 20.2° 2θ were detected for Li-Al LDH-CO_3^{2-}/OH^- CC. Comparing two Li-Al LDH CCs, the reflections of bayerite were significantly more intensive for the specimen prepared in the absence of NH_4OH. This result also indicates the presence of lower amount of corrosion products on the surface of 0.1–11.5–30–24–**NH_4OH**.

4. Discussion

In order to understand how synthesis conditions affect the process of the Li-Al LDH-CO_3^{2-}/OH^- CC crystallisation on the surface of AA2024 aluminium alloy, concentration of lithium carbonate, pH of the solution, temperature of the synthesis and treatment time were systematically varied. Additionally, the chelating agent was applied for the synthesis. Increase of Li_2CO_3 concentration in the reaction mixture from 0.05 to 0.15 M resulted of the formation of non-uniform coating made of disordered LDH flakes with broad size distribution. It indicates that the range of concentrations, which is sufficient to form the homogenous coating on the surface of AA2024, was limited by 0.1 M Li_2CO_3. Such observation differs from our previous results devoted to the preparation of Zn-Al LDH CC, whose homogenous crystallisation was reached only from high concentrated reaction bathes.

Variation of the treatment time from 15 min till 30 h (at 30 °C)

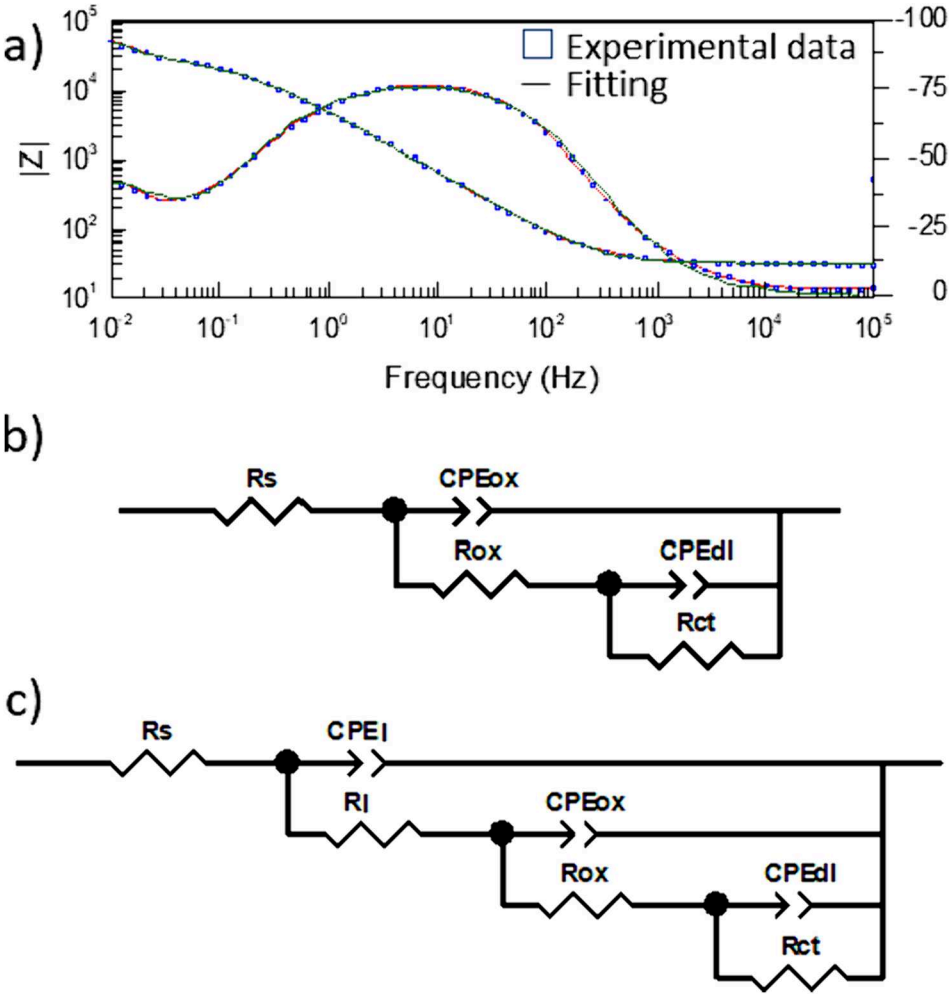

Fig. 9. A) An example of the fitting of experimental impedance spectrum (CC obtained with 0.1 M Li_2CO_3 at pH = 11.5 at 30 °C for 24 h in the presence of NH_4OH after 24 h of EIS) and the equivalent circuits used to model the impedance data for b) all specimens except c) 0.1–11.5–30–24–**NH_4OH** after 1 h of EIS (3.5 wt% NaCl, 25 °C).

demonstrated that formation of Li-Al LDH-CO_3^{2-}/OH^- CC can be achieved only at longer treatment times, i.e. 24 h, but no further difference was detected for further prolongation to 30 h. This behaviour was associated with the mechanism and kinetics of the process of LDH formation. For the Li-Al LDH coating, lithium ions are provided into the coating from the reaction bath, while aluminium is delivered into the coating in the process of the direct dissolution of the AA2024 substrate. As it was demonstrated by the several works of Visser, the process of Li-Al LDH growth on the surface of AA2024 alloy is complex and includes several stages: thinning of native oxide, formation of $Al(OH)_3$ followed by intercalation of lithium ions insight aluminium hydroxide and transformation into Li-Al LDH [41,67]. While under high pH (>11), the first two processes run relatively fast, the process of lithium intercalation is slow. As a result, altogether, the formation of homogeneous Li-Al LDH CC takes longer.

The optimum pH for the formation of Li-Al LDH-CO_3^{2-}/OH^- CC was found in the range of 10.5–11.5. Further increase of the pH to 12 led to the cracking of the surface and deposition of agglomerated Cu-rich intermetallics on the upper surface of the coating. Consequently, it resulted in further loss of Li-Al LDH CC protective ability as the surface cracks provided easy pathways for corrosion media to the metallic interface. In turn, intermetallics represent high efficient Cu cathodes to start the corrosion process.

Impact of temperature on LDH formation was also observed, when it was increased from 30 to 50 °C. The specimens obtained under 50 °C demonstrated enhanced protective ability compared to one under 30 °C, which was related to the structure differences in Li-Al LDH-CO_3^{2-}/OH^- CC. The CC layer prepared at 50 °C was thicker and formed by the LDH flakes with higher crystals size compared to the one obtained under 30 °C, and consequently formed higher physical barrier on the surface, which was demonstrated by cross section and EDS analyses. Moreover, in contrast to 0.1–11.5–30–24, the coating prepared at 50 °C contained the admixtures of $Al(OH)_3$ and $5Al_2O_3{\cdot}H_2O$ phases, which can also affect the protective ability of AA2024 aluminium alloy.

Among all conditions varied, involvement of NH_4OH as chelating agent had the highest impact on the protective ability of the final Li-Al LDH-CO_3^{2-}/OH^- CC. This coating demonstrated the highest corrosion resistance, which remained stable for 168 h of EIS. Regardless of the fact that no principal differences were detected in the LDH structure by XRD, SEM and Raman spectroscopy comparing to the specimen obtained under the same condition without chelating agent, the improved protection ability was related to microstructure properties of the final materials, apparently distribution of copper on the surface. It was controlled by the presence of NH_4OH, whose functions must be mentioned. First, NH_4OH presented in the reaction bath can facilitate the dissolution of copper from the intermetallic particles similarly to reported in [30]. The favoured dissolution of Cu takes place due to an electrochemical process, where the cathodic reaction is the reduction of oxygen at the surface and the anodic reaction is the oxidation of Cu [68]. After that, the released copper forms soluble complexes with ammonia,

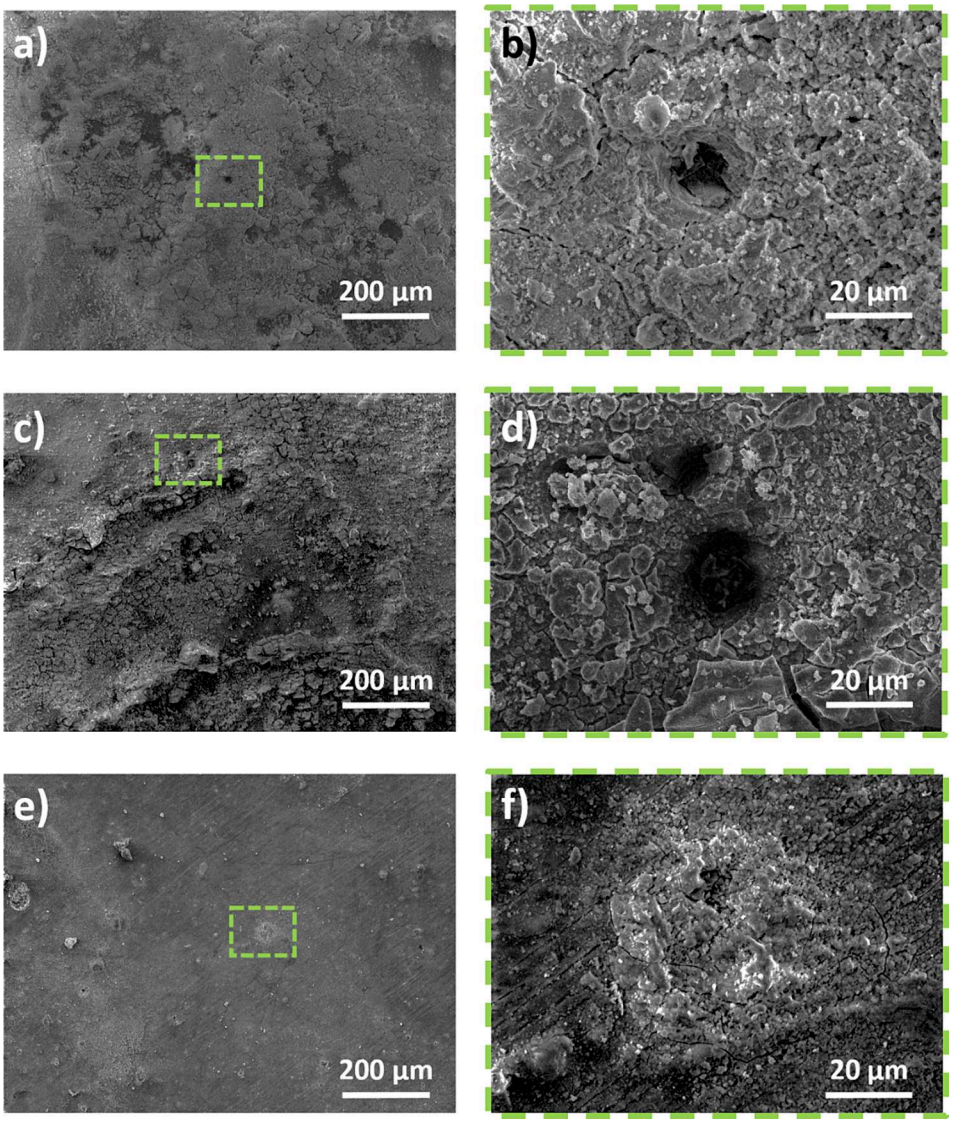

Fig. 10. SEM picture of the specimens after SST test for 168 h: a)-b) bare AA2024 aluminium alloy and one coated with Li-Al LDH-CO_3^{2-}/OH^-: c)-d) 0.1–11.5–30–24 and e)-f) 0.1–11.5–30–24–**NH_4OH**.

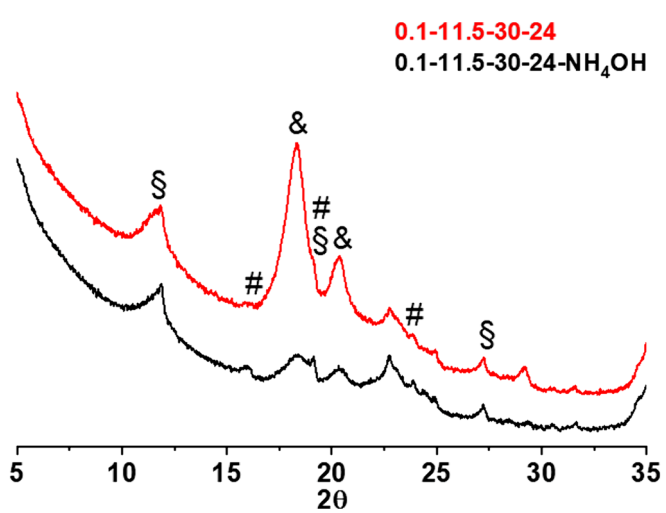

Fig. 11. XRD patterns of the Li-Al LDH-CO_3^{2-}/OH^- CC after SST test for 168 h. &-$Al(OH)_3$ (bayerite), #-Al_2O_3, § -AA2024.

e.g. $Cu(NH_3)_x^{2+}$ [69]. In turn, it prevents further redeposition of Cu species on the surface, which can lead to the generation of significantly more efficient Cu cathodes comparing to intermetallic particles of AA2024 alloy [30]. This assumption correlates with the results of GDOES, which demonstrated lower amount of Cu in the LDH layer prepared in the presence of ammonia, while for the other specimens more copper was located in the coating region. Additionally, to confirm the assumption about possible Cu species redeposition, thermodynamic calculation were performed by Hydra-Medusa software (SI, *Fig. SI-12*). Thus, soluble $Cu(NH_3)^+$ is dominating Cu specie present in the range of pH from 7 till 12 in the presence of ammonia, while without NH_3 it is insoluble Cu_2O. Moreover, ammonia present in the solution can provide the local pH buffering close to the interface [70].

Table 3 sums up the impact of the synthesis parameters mentioned previously on protective ability of the Li-Al LDH-CO_3^{2-}/OH^- CC.

Based on the obtained results, the following mechanism of protection can be proposed for Li-Al LDH-CO_3^{2-}/OH^- CC (Fig. 12). For LDH-coated samples, LDH-flakes act firstly as physical barrier against the aggressive anions of the solution like Cl^- as it is schematically presented in (Fig. 12, a). In that context, the corrosion resistance is related to the size of LDH-flakes and their orientation and consequently the thickness of the LDH layer on the substrate. The thicker and more homogeneous the LDH

Table 3
Parameters of Li-Al LDH-CO_3^{2-}/OH^- CC growth on AA2024 alloy and their impact on the protective properties of the final coating.

Factor	c(Li_2CO_3)	pH	Temperature	Time	Chelating agent
Impact on corrosion protection	±	+	+	±	++
Tested conditions	0.05–0.15 M	6–12	30–50 °C	1–36 h	NH_4OH (pH = 11.5)
Optimal conditions	0.1 M	10.5–11.5	50 °C	24 h	NH_4OH (pH = 11.5)
Reason	Disorder of LDH flakes on the surface for syntheses with 0.15 M Li_2CO_3	Favourable dissolution of native oxide at basic pH	Accelerated growth of LDH crystals at higher temperatures, but formation of admixture phases	Slow integration of lithium insight Al $(OH)_3$	Chelating of Cu and prevention of its further redeposition

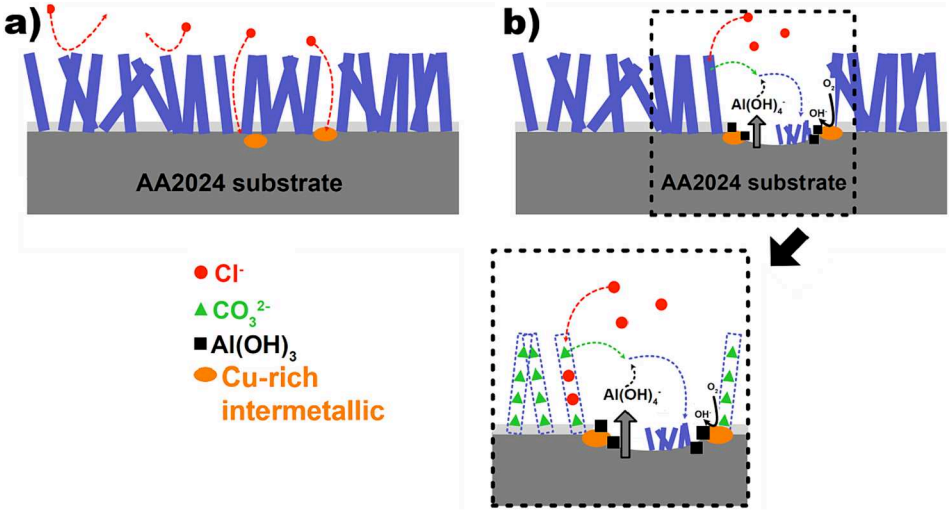

Fig. 12. Schematic diagram of corrosion resistance mechanism of the Li-Al LDH-CO_3^{2-}/OH^- CC coated AA2024 Al alloy in 3.5 wt% NaCl solution: a) schematic representation of barrier protection, b) representation of ion-exchange ability and self-healing properties of the coating.

coating is, the better corrosion resistance should be. Another function of LDH flakes consist in the capture of chloride and release carbonate anions (Fig. 12, b, insert). However, this process is slow and limited due to the low ability of CO_3^{2-} to be exchanged by Cl^- [71]. Nevertheless, after the long-term exposure in aggressive media, some chloride anions reach the surface of aluminium alloy and provoke the process of corrosion, which start mainly on the Cu-rich intermetallic particles. In this context, the coatings prepared without chelating agent are more susceptible to corrosion due to the presence of higher amount of redeposited copper containing intermetallics on the surface. Reduction of the oxygen on the Cu-rich particles results in an increase of the local pH, followed by the dissolution of native oxide and the substrate and formation of $Al(OH)_3$. Being insoluble, aluminium hydroxide deposits on the metallic surface forming an additional protective barrier. However, protective ability of this layer is limited, as $Al(OH)_3$ can be further transformed into soluble $Al(OH)_4^-$ at high pH. Discussing protective ability of Li-Al LDH, another possible aspect should be mentioned. The processes taking place on the surface can cause also Li-Al LDH degradation leading to release of Li^+ ions into the media. In turn, they can further react with $Al(OH)_4^-$ forming new LDH flakes (Fig. 12, b) on the surface similarly to the processes represented in [40–44,49,63,67,72]. The formation of new flakes allows the coating to repair itself and reach again its level of protection.

Finally, it must be mentioned, that lithium carbonate belongs to the compounds, whose production is controlled by REACH regulations. Thus, further development of cheap and environmentally friendly conversion coatings is still required. As alternatives to Li-Al LDH, Mg-Al LDH and Ca-Al LDH can be considered. However, currently most of the reported methods for preparation of these LDHs are based on the hydrothermal syntheses in autoclaves [73–76], whose application is problematic especially on industrial level. In that context, fast ways of the syntheses of Ca-Al and Mg-Al LDH on the surface of aluminium alloys under mild conditions should be developed. Moreover, search of environmentally friendly chelating agent for Cu-rich intermetallics is an important direction for the development high protective LDH based CC for AA2024 alloy.

5. Conclusions

This article contributes to the understanding of the protective ability of Li-Al LDH-CO_3^{2-}/OH^- CC grown on the surface of AA2024 aluminium alloy and how it can be modified through the variation of the synthesis parameters. For this purpose concentration of lithium carbonate, pH of the solution, temperature and treatment time were systematically varied. Additionally to that, Li-Al LDH crystallisation in the presence of NH_4OH was performed. Variation of **Li_2CO_3 concentration** in the range from 0.05 to 0.15 M demonstrated that the coating with homogenous covering with Li-Al LDH flakes was formed from the reaction mixture containing **0.1 M Li_2CO_3**. In turn, the compact LDH layer was formed in the range of **pH = 10–11.5,** which is explained by facilitation of the native oxide dissolution in alkaline media. Due to slow incorporation of lithium ions into $Al(OH)_4^-$, homogenous coverage of the surface with Li-Al LDH flakes can be achieved only after longer treatment time (**24 h** at 30 °C). In terms of the **temperature** role, more protective coatings were obtained at **50 °C**. It was associated with the acceleration of the LDH growth at higher T °C, and consequently the formation of the thicker layer with higher barrier ability. Among all varied parameters, **addition of chelating agent in the LDH reaction mixture** was the most effective. The Li-Al LDH-CO_3^{2-}/OH^- CC prepared in the presence of **NH_4OH**

demonstrated the highest level of corrosion resistance. It was related to the interface homogenisation, effect of ammonia on the local pH buffering close to the interface and prevention of Cu species redeposition, which was released from intermetallics during the LDH synthesis, through the formation of its soluble complexes with NH_4OH.

CRediT authorship contribution statement

Jules Stephan: Writing – original draft, Visualization, Investigation, Formal analysis. **Valeryia Kasneryk:** Writing – original draft, Visualization, Supervision, Methodology, Investigation, Formal analysis, Conceptualization. **Maria Serdechnova:** Writing – review & editing, Conceptualization. **Nico Scharnagl:** Writing – review & editing, Investigation. **Eugen Gazenbiller:** Writing – review & editing, Investigation. **Bahram Vaghefinazari:** Investigation. **Polina Volovitch:** Writing – review & editing, Data curation. **Maksim Starykevich:** Writing – review & editing, Visualization, Investigation. **Carsten Blawert:** Writing – review & editing, Supervision, Conceptualization. **Mikhail L. Zheludkevich:** Writing – review & editing, Supervision, Project administration.

Declaration of competing interest

The authors declare that they have no known competing financial interests or personal relationships that could have appeared to influence the work reported in this paper.

Data availability

No data was used for the research described in the article.

Acknowledgements

This investigation was carried out with the financial support of the COVER project in frame of LUFO V-3 Call 2018. The authors thank to Dr. Silke Grünke and Dr. Stefan Kreling from Airbus (Germany) and Dr. Markus Becker from Fraunhofer IFAM (Germany). Dr. Valeryia Kasneryk thanks Alexander von Humboldt Foundation (Germany) and Christiane Nüsslein-Volhard Foundation (Germany) for financial support. Dr. Maksim Starykevich acknowledges the support of the FCT–2020.00625. CEECIND (Portugal) grant. The authors thank to Daniel Strerath for spark analysis. The authors are also grateful to Deutsches Elektronen-Synchrotron PETRA III (Hamburg, Germany) for accepting and granting the proposal I-20211324 (P.08 end-station) and Dr. Florian Wieland and Dr. Vasyl M. Haramus for the experimental support during DESY beamline experiments. Finally, the authors thank to Mr. Volker Heitmann, Mr. Ulrich Burmester and Mr. Thymoty Naacke for technical support during the investigations.

Appendix A. Supplementary material

Supplementary data to this article can be found online at https://doi.org/10.1016/j.apsusc.2024.159919.

References

[1] D. Varshney, K. Kumar, Application and use of different aluminium alloys with respect to workability, strength and welding parameter optimization, Ain Shams Eng. J. 12 (2021) 1143–1152.
[2] T. Hashimoto, X. Zhang, X. Zhou, P. Skeldon, S.J. Haigh, G.E. Thompson, Investigation of dealloying of S phase (Al_2CuMg) in AA 2024–T3 aluminium alloy using high resolution 2D and 3D electron imaging, Corros. Sci. 103 (2016) 157–164.
[3] A. Boag, A.E. Hughes, A.M. Glenn, T.H. Muster, D. McCulloch, Corrosion of AA2024-T3 Part I: localised corrosion of isolated IM particles, Corros. Sci. 53 (2011) 17–26.
[4] B. Minhas, S. Dino, L. Huang, D. Wu, Active corrosion protection by epoxy coating on Li_2CO_3-pretreated anodized aluminum alloy 2024–T3, Front. Mater. 8 (2022).
[5] A.M. Glenn, T.H. Muster, C. Luo, X. Zhou, G.E. Thompson, A. Boag, A.E. Hughes, Corrosion of AA2024-T3 Part III: propagation, Corros. Sci. 53 (2011) 40–50.
[6] H. Wei, J. Xia, W. Zhou, L. Zhou, G. Hussain, Q. Li, K. Ostrikov, Adhesion and cohesion of epoxy-based industrial composite coatings, Compos. B Eng. 193 (2020) 108035.
[7] A.C. Bouali, M. Serdechnova, C. Blawert, J. Tedim, M.G.S. Ferreira, M. L. Zheludkevich, Layered double hydroxides (LDHs) as functional materials for the corrosion protection of aluminum alloys: a review, Appl. Mater. Today 21 (2020) 100857.
[8] A. Stankiewicz, I. Szczygieł, B. Szczygieł, Self-healing coatings in anti-corrosion applications, J. Mater. Sci. 48 (2013) 8041–8051.
[9] F. Zhang, P. Ju, M. Pan, D. Zhang, Y. Huang, G. Li, X. Li, Self-healing mechanisms in smart protective coatings: a review, Corros. Sci. 144 (2018) 74–88.
[10] C. Pellerin, S.M. Booker, Reflections on hexavalent chromium: health hazards of an industrial heavyweight, Environ Health Perspect 108 (2000) A402–A407.
[11] F. Peltier, D. Thierry, Review of Cr-free coatings for the corrosion protection of aluminum aerospace alloys, Coatings 12 (2022) 518.
[12] R.L. Twite, G.P. Bierwagen, Review of alternatives to chromate for corrosion protection of aluminum aerospace alloys, Prog. Org. Coat. 33 (1998) 91–100.
[13] M.A. Iqbal, L.Y. Sun, A.T. Barrett, M. Fedel, Layered double hydroxide protective films developed on aluminum and aluminum alloys: synthetic methods and anti-corrosion mechanisms, Coatings 10 (2020) 428.
[14] D. Tonelli, I. Gualandi, E. Musella, E. Scavetta, Synthesis and Characterization of Layered Double Hydroxides as Materials for Electrocatalytic Applications, Nanomaterials 11 (2021) 725.
[15] A.I. Khan, D. O'Hare, Intercalation chemistry of layered double hydroxides: recent developments and applications, J. Mater. Chem. 12 (2002) 3191–3198.
[16] Y. Kuang, L. Zhao, S. Zhang, F. Zhang, M. Dong, S. Xu, Morphologies Preparations and Applications of Layered Double Hydroxide Micro-/nanostructures, Materials 3 (2010) 5220–5235.
[17] V. Kasneryk, M. Serdechnova, C. Blawert, M.L. Zheludkevich, LDH has been grown: what is next? Overview on Methods of Post-Treatment of LDH Conversion Coatings, Appl. Clay Sci. 232 (2023) 106774.
[18] A.C. Bouali, M.H. Iuzviuk, M. Serdechnova, K.A. Yasakau, D.C.F. Wieland, G. Dovzhenko, H. Maltanava, I.A. Zobkalo, M.G.S. Ferreira, M.L. Zheludkevich, Zn-Al LDH growth on AA2024 and zinc and their intercalation with chloride: Comparison of crystal structure and kinetics, Appl. Surf. Sci. 501 (2020) 144027.
[19] J. Tedim, M.L. Zheludkevich, A.N. Salak, A. Lisenkov, M.G.S. Ferreira, Nanostructured LDH-container layer with active protection functionality, J. Mater. Chem. 21 (2011) 15464–15470.
[20] J. Tedim, A.C. Bastos, S. Kallip, M.L. Zheludkevich, M.G.S. Ferreira, Corrosion protection of AA2024-T3 by LDH conversion films, Analysis of SVET Results, Electrochimica Acta 210 (2016) 215–224.
[21] J. Tedim, M.L. Zheludkevich, A.C. Bastos, A.N. Salak, A.D. Lisenkov, M.G. S. Ferreira, Influence of preparation conditions of layered double hydroxide conversion films on corrosion protection, Electrochim. Acta 117 (2014) 164–171.
[22] J. Tedim, M.L. Zheludkevich, A.C. Bastos, A.N. Salak, J. Carneiro, F. Maia, A. D. Lisenkov, A.B. Oliveira, M.G.S. Ferreira, Effect of Surface Treatment on the Performance of LDH Conversion Films, ECS Electrochemistry Letters 3 (2014) C4–C8.
[23] Y. Zhang, J.H. Liu, Y.D. Li, M. Yu, S.M. Li, B. Xue, Fabrication of inhibitor anion-intercalated layered double hydroxide host films on aluminum alloy 2024 and their anticorrosion properties, J. Coat. Technol. Res. 12 (2015) 293–302.
[24] C.S. Neves, A.C. Bastos, A.N. Salak, M. Starykevich, D. Rocha, M.L. Zheludkevich, A. Cunha, A. Almeida, J. Tedim, M.G.S. Ferreira, Layered double hydroxide clusters as precursors of novel multifunctional layers: a bottom-up approach, Coatings 9 (2019) 328.
[25] Y. Zhang, P.H. Yu, J.P. Wang, Y.D. Li, F. Chen, K. Wei, Y. Zuo, LDHs/graphene film on aluminum alloys for active protection, Appl. Surf. Sci. 433 (2018) 927–933.
[26] J. Li, B. Hurley, R. Buchheit, Inhibition performance study of vanadate on AA2024-T3 at high temperature by SEM FIB, Raman and XPS, J. Electrochem. Soc. 162 (2015) C219.
[27] K. Wei, X. Zhao, Z. Zhang, Y. Yuan, W. Kong, Y. Zhang, Duplex Coating Combing Vanadate-Intercalated Layered Double Hydroxide and Ce-doped Sol-Gel Layers on Aluminum Alloy for Active Corrosion Protection, Materials 16 (2023) 775.
[28] I. Milošev, Corrosion inhibition of aluminium alloys by molybdate ions: a critical review of the chemistry, mechanisms and applications, Corros. Sci. 229 (2024) 111854.
[29] A.C. Balaskas, M. Curioni, G.E. Thompson, Corrosion protection mechanism of 2-mercaptobenzothiazole and its potential synergistic effect with cerium ions for treatment of AA 2024–T3, J. Electroanal. Chem. 863 (2020) 114081.
[30] A.C. Bouali, M. Serdechnova, K.A. Yasakau, A. Lutz, G. Wiese, H. Terryn, M.G. S. Ferreira, M.L. Zheludkevich, The role of Cu-based Intermetallic on the direct growth of a ZnAl LDH film on AA2024, J. Electrochem. Soc. 169 (2022) 081501.
[31] K.A. Yasakau, A. Kuznetsova, S. Kallip, M. Starykevich, J. Tedim, M.G.S. Ferreira, M.L. Zheludkevich, A novel bilayer system comprising LDH conversion layer and sol-gel coating for active corrosion protection of AA2024, Corros. Sci. 143 (2018) 299–313.
[32] I. Mohammadi, T. Shahrabi, M. Mahdavian, M. Izadi, A novel corrosion inhibitive system comprising Zn-Al LDH and hybrid sol-gel silane nanocomposite coating for AA2024-T3, J. Alloy. Compd. 909 (2022) 164755.
[33] R.G. Buchheit, M.D. Bode, G.E. Stoner, Corrosion-resistant, chromate-free talc coatings for aluminum, Corrosion 50 (1994) 205–214.
[34] C.X. Zhang, X.H. Luo, X.Y. Pan, L.Y. Liao, X.S. Wu, Y.L. Liu, Self-healing Li-Al layered double hydroxide conversion coating modified with aspartic acid for 6N01 Al alloy, Appl. Surf. Sci. 394 (2017) 275–281.

[35] K. Lin, X. Luo, X. Pan, C. Zhang, Y. Liu, Enhanced corrosion resistance of LiAl-layered double hydroxide (LDH) coating modified with a schiff base salt on aluminum alloy by one step in-situ synthesis at low temperature, Appl. Surf. Sci. 463 (2019) 1085–1096.
[36] J. Ma, M. Chang, H. He, H. Wei, Y. Huang, X. Du, D. Chen, Corrosion resistance of Li-Al LDHs film modified by methionine for 6063 Al alloy in 3.5 wt.% NaCl solution, Coatings 12 (2022) 507.
[37] B. Yang, Y. Ma, Z. Liang, Y. Liao, Z. Wang, P. Zhu, A superhydrophobic and corrosion resistant layered double hydroxides coating on AA2099-T83 Al-Cu-Li alloy, Surf. Coat. Technol. 405 (2021) 126629.
[38] Y. Zhang, J.H. Liu, Y.D. Li, M. Yu, S.M. Li, B. Xue, A facile approach to superhydrophobic LiAl-layered double hydroxide film on Al-Li alloy substrate, J. Coat. Technol. Res. 12 (2015) 595–601.
[39] J. Li, T.C. Yuan, C.L. Zhou, B. Chen, Y. Shuai, D.W. Wu, D.C. Chen, X.H. Luo, Y. F. Cheng, Y.L. Liu, Facile Li-Al layered double hydroxide films on Al alloy for enhanced hydrophobicity, anti-biofouling and anti-corrosion performance, J. Mater. Sci. Technol. 79 (2021) 230–242.
[40] P. Visser, Y. Liu, H. Terryn, J.M.C. Mol, Lithium salts as leachable corrosion inhibitors and potential replacement for hexavalent chromium in organic coatings for the protection of aluminum alloys, J. Coat. Technol. Res. 13 (2016) 557–566.
[41] P. Visser, Y. Liu, X. Zhou, T. Hashimoto, G.E. Thompson, S.B. Lyon, L.G.J. van der Ven, A.J.M.C. Mol, H.A. Terryn, The corrosion protection of AA2024-T3 aluminium alloy by leaching of lithium-containing salts from organic coatings, Faraday Discuss. 180 (2015) 511–526.
[42] P. Visser, A. Lutz, J.M.C. Mol, H. Terryn, Study of the formation of a protective layer in a defect from lithium-leaching organic coatings, Prog. Org. Coat. 99 (2016) 80–90.
[43] P. Visser, M. Meeusen, Y. Gonzalez-Garcia, H. Terryn, J.M.C. Mol, Electrochemical evaluation of corrosion inhibiting layers formed in a defect from lithium-leaching organic coatings, J. Electrochem. Soc. 164 (2017) C396.
[44] E. Michailidou, P. Visser, J.M.C. Mol, A. Kosari, H. Terryn, K. Baert, Y. Gonzalez-Garcia, The effect of pH on the corrosion protection of aluminum alloys in lithium-carbonate-containing NaCl solutions, Corros. Sci. 210 (2023) 110851.
[45] R.R. Miller, S.H. Smith, D.D. Williams, Solubility of lithium carbonate at elevated temperatures, J. Chem. Eng. Data 16 (1971) 74–75.
[46] Puigdomenech I., HydraMedusa Software, KTH Royal Institut of Technology, (2015) https://www.kth.se/che/medusa/downloads-1.386254.
[47] S.-L. Wang, C.-H. Lin, Y.-Y. Yan, M.K. Wang, Synthesis of Li/Al LDH using aluminum and LiOH, Appl. Clay Sci. 72 (2013) 191–195.
[48] D. Mata, M. Serdechnova, M. Mohedano, C.L. Mendis, S.V. Lamaka, J. Tedim, T. Hack, S. Nixon, M.L. Zheludkevich, Hierarchically organized Li-Al-LDH nano-flakes: a low-temperature approach to seal porous anodic oxide on aluminum alloys, RSC Adv. 7 (2017) 35357–35367.
[49] A. Kosari, F. Tichelaar, P. Visser, P. Taheri, H. Zandbergen, H. Terryn, J.M.C. Mol, Nanoscopic and in-situ cross-sectional observations of Li-based conversion coating formation using liquid-phase TEM, npj Mater. Degrad. 5 (2021) 40.
[50] Y.-X. Zhu, G.-L. Song, D.-J. Zheng, M. Serdechnova, C. Blawert, M.L. Zheludkevich, In situ synergistic strategy of sacrificial intermedium for scalable-manufactured and controllable layered double hydroxide film, Sci. China Mater. 65 (2022) 1842–1852.
[51] O. Gharbi, N. Birbilis, K. Ogle, In-situ monitoring of alloy dissolution and residual film formation during the pretreatment of Al-alloy AA2024-T3, J. Electrochem. Soc. 163 (2016) C240.
[52] J.T. Kloprogge, D. Wharton, L. Hickey, R.L. Frost, Infrared and Raman study of interlayer anions CO_3^{2-}, NO_3^-, SO_4^{2-} and ClO_4^- in Mg/Al-hydrotalcite, Am. Mineral. 87 (2002) 623–629.
[53] C. Luciano Honorato, C. Sandra Shirley Ximeno, L. Alexandre Amaral, D. Renata, Raman Spectroscopy for Characterization of Hydrotalcite-like Materials Used in Catalytic Reactions, in: P. Chandra Shakher, K. Samir (Eds.) Recent Developments in Atomic Force Microscopy and Raman Spectroscopy for Materials Characterization, IntechOpen, Rijeka, 2021, pp. Ch. 8.
[54] T. Shulha, M. Serdechnova, M.H. Iuzviuk, I.A. Zobkalo, P. Karlova, N. Scharnagl, D. C.F. Wieland, S.V. Lamaka, A.A. Yaremchenko, C. Blawert, M.L. Zheludkevich, In situ formation of LDH-based nanocontainers on the surface of AZ91 magnesium alloy and detailed investigation of their crystal structure, J. Magnesium Alloys 10 (2021) 1268–1285.
[55] F. Theiss, A. López, R.L. Frost, R. Scholz, Spectroscopic characterisation of the LDH mineral quintinite $Mg_4Al_2(OH)_{12}CO_3{\cdot}3H_2O$, Spectrochim. Acta A Mol. Biomol. Spectrosc. 150 (2015) 758–764.
[56] I. Mohammadi, T. Shahrabi, M. Mahdavian, M. Izadi, Zn-Al layered double hydroxide as an inhibitive conversion coating developed on AA2024-T3 by one-step hydrothermal crystallization: crystal structure evolution and corrosion protection performance, Surf. Coat. Technol. 409 (2021) 126882.
[57] A.C. Bouali, M.H. Iuzviuk, M. Serdechnova, K.A. Yasakau, D. Drozdenko, A. Lutz, K. Fekete, G. Dovzhenko, D.C.F. Wieland, H. Terryn, M.G.S. Ferreira, I.A. Zobkalo, M.L. Zheludkevich, Mechanism of LDH Direct Growth on Aluminum Alloy Surface: A Kinetic and Morphological Approach, J. Phys. Chem. C 125 (2021) 11687–11701.
[58] K.A. Yasakau, M.L. Zheludkevich, S.V. Lamaka, M.G.S. Ferreira, Mechanism of Corrosion Inhibition of AA2024 by Rare-Earth Compounds, J. Phys. Chem. B 110 (2006) 5515–5528.
[59] R.G. Buchheit, M.A. Martinez, L.P. Montes, Evidence for Cu ion formation by dissolution and dealloying the Al_2CuMg Intermetallic compound in rotating ring-disk collection Experiments, J. Electrochem. Soc. 147 (2000) 119.
[60] G. Williams, A.J. Coleman, H.N. McMurray, Inhibition of aluminium alloy AA2024-T3 pitting corrosion by copper complexing compounds, Electrochim. Acta 55 (2010) 5947–5958.
[61] A. Boag, R.J. Taylor, T.H. Muster, N. Goodman, D. McCulloch, C. Ryan, B. Rout, D. Jamieson, A.E. Hughes, Stable pit formation on AA2024-T3 in a NaCl environment, Corros. Sci. 52 (2010) 90–103.
[62] Y. Liu, T.W. Yu, R. Cai, Y.S. Li, W.S. Yang, J.G. Caro, One-pot synthesis of NiAl-CO_3 LDH anti-corrosion coatings from CO_2-saturated precursors, RSC Adv. 5 (2015) 29552–29557.
[63] A. Kosari, P. Visser, F. Tichelaar, S. Eswara, J.N. Audinot, T. Wirtz, H. Zandbergen, H. Terryn, J.M.C. Mol, Cross-sectional characterization of the conversion layer formed on AA2024-T3 by a lithium-leaching coating, Appl. Surf. Sci. 512 (2020) 145665.
[64] I. Mohammadi, T. Shahrabi, M. Mahdavian, M. Izadi, Chemical modification of LDH conversion coating with diethyldithiocarbamate as a novel anti-corrosive film for AA2024-T3, J. Ind. Eng. Chem. 95 (2021) 134–147.
[65] Y. Zhang, Y.D. Li, Y.S. Ren, H. Wang, F. Chen, Double-doped LDH films on aluminum alloys for active protection, Mater. Lett. 192 (2017) 33–35.
[66] R. del Olmo, M. Mohedano, E. Matykina, R. Arrabal, Permanganate loaded Ca-Al-LDH coating for active corrosion protection of 2024–T3 alloy, Corros. Sci. 198 (2022) 110144.
[67] P. Visser, Y. Gonzalez-Garcia, J.M.C. Mol, H. Terryn, Mechanism of Passive Layer Formation on AA2024-T3 from Alkaline Lithium Carbonate Solutions in the Presence of Sodium Chloride, J. Electrochem. Soc. 165 (2018) C60–C70.
[68] D. Strmčnik, M. Gaberšček, B. Pihlar, D. Kočar, J. Jamnik, Copper dissolution in ammonia solutions: identification of the mechanism at low overpotentials, J. Electrochem. Soc. 156 (2009) C222.
[69] A.R. Johnson, T.M. McQueen, K.T. Rodolfa, Species distribution diagrams in the copper-ammonia system: an updated and expanded demonstration illustrating complex equilibria, J. Chem. Educ. 82 (2005) 408.
[70] M.C. Ribeiro, A.C. Frank, P.T.A. Sumodjo, The influence of ammonia on the electroless deposition of CoB alloys from alkaline citrate containing baths, Electrochim. Acta 147 (2014) 752–757.
[71] S. Miyata, Anion-exchange properties of hydrotalcite-like compounds, Clay Clay Miner. 31 (1983) 305–311.
[72] Z. Li, P. Visser, A.E. Hughes, A. Homborg, Y. Gonzalez-Garcia, A. Mol, Review of the state of art of Li-based inhibitors and coating technology for the corrosion protection of aluminium alloys, Surf. Coat. Technol. 478 (2024) 130441.
[73] W. Wu, F. Zhang, Y.C. Li, Y.F. Zhou, Q.S. Yao, L. Song, R.C. Zeng, S.C. Tjong, D. C. Chen, Corrosion resistance of a silane/ceria modified Mg-Al-layered double hydroxide on AA5005 aluminum alloy, Frontiers of, Mater. Sci. 13 (2019) 420–430.
[74] F.Y. Wang, Z.G. Guo, Insitu growth of durable superhydrophobic Mg-Al layered double hydroxides nanoplatelets on aluminum alloys for corrosion resistance, J. Alloy. Compd. 767 (2018) 382–391.
[75] M.A. Iqbal, L. Sun, M. Fedel, Synthesis of novel cone-shaped CaAl-LDH directly on aluminum alloy by a facile urea hydrolysis method, SN Applied Sciences 1 (2019) 1415.
[76] M.A. Iqbal, L.Y. Sun, A.M. LaChance, H. Ding, M. Fedel, In situ growth of a CaAl-NO_3layered double hydroxide film directly on an aluminum alloy for corrosion resistance, Dalton Trans. 49 (2020) 3956–3964.